Lithos 119 (2010) 313–329

Contents lists available at ScienceDirect

Lithos

journal homepage: www.elsevier.com/locate/lithos

The early Jurassic mafic–ultramafic intrusion and A-type granite from northeastern Guangdong, SE China: Age, origin, and tectonic significance

Wei-Guang Zhu [a,*], Hong Zhong [a], Xian-Hua Li [b], De-Feng He [a], Xie-Yan Song [a], Tao Ren [a], Zhong-Quan Chen [c], Hui-Si Sun [d], Jin-Qing Liao [d]

[a] State Key Laboratory of Ore Deposit Geochemistry, Institute of Geochemistry, Chinese Academy of Sciences, 46 Guanshui Road, Guiyang 550002, China
[b] State Key Laboratory of Lithospheric Evolution, Institute of Geology and Geophysics, Chinese Academy of Sciences, P.O. Box 9825, Beijing 100029, China
[c] Foshan Geological Bureau of Guangdong Province, Foshan 528000, China
[d] Geological Team 723, Bureau of Geology and Mineral Resources of Guangdong Province, Meizhou 514089, China

ARTICLE INFO

Article history:
Received 3 December 2009
Accepted 11 July 2010
Available online 21 July 2010

Keywords:
Early Jurassic
Mafic–ultramafic intrusion
A-type granites
SE China

ABSTRACT

The early Yanshanian geology of Southeastern (SE) China is characterized by widespread igneous rocks consisting predominantly of granites and rhyolites, and subordinate mafic intrusive and volcanic rocks. However, the onset time, petrogenesis, and tectonic implications of the early Jurassic magmatism in SE China remain highly controversial. We report here zircon U–Pb ages, geochemistry, and Nd–Sr isotopic data for the Fe–Ti–V oxide-bearing Xianlan mafic–ultramafic intrusion and the Wengong granitic pluton in northeast Guangdong. SHRIMP and Cameca SIMS U–Pb zircon ages indicate that the Xialan gabbros and the Wengong granites were emplaced at 194 ± 1 Ma and 192 ± 1 Ma, respectively. Although the field observations show that the granitic pluton intruded the mafic–ultramafic intrusion, the dating results suggest that they were formed almost contemporaneously.

The ore-barren gabbros of the Xialan intrusion are commonly high in Fe_2O_3, CaO and Al_2O_3 contents, with variable SiO_2, TiO_2, and MgO contents. In contrast, the Fe–Ti–V-bearing gabbros have higher Fe_2O_3, TiO_2 (3.5–5.4%) and V contents. These gabbros with high $\varepsilon_{Nd}(T)$ values (+1.7 to +6.2) and low initial I_{Sr} values (0.704 to 0.706), are characterized by LREE-enriched and "convex upwards" incompatible trace-element patterns with slightly negative Nb–Ta anomalies. The parental magma for the gabbros exhibits affinity with a high-Ti subalkaline basaltic magma generated by melting of a depleted OIB-like mantle source. We suggest that the gabbros originated by fractional crystallization of the parental magma plus varying degrees of crustal contamination.

The Wengong granites have high SiO_2 and ($Na_2O + K_2O$) contents, are LREE-enriched and show relatively flat-HREE patterns and significantly negative Eu, Nb, Sr, P and Ti anomalies in the primitive mantle-normalized spidergrams. These granitic rocks display geochemical characteristics of A_2-type granites including high FeO^T/MgO ratios (7.6–14.7), elevated high-field-strength element (HFSE) contents, and high Ga/Al ratios (2.75–3.49). The Wengong granites exhibit variably initial $\varepsilon_{Nd}(T)$ values ranging from −2.8 to +1.2, whereas the initial I_{Sr} values show large uncertainties due to relatively high Rb/Sr ratios. The parental magma for these rocks exhibits affinity with a mildly alkaline magma, which was probably generated by partial melting of the regional Paleoproterozoic amphibolites and thereafter mixed with various amounts of the early Jurassic basaltic magmas. The granites were then formed by extensive crystal fractionation of the mildly alkaline magma.

The Xialan mafic–ultramafic intrusion and the Wengong granitic pluton were formed in an anorogenic extensional environment. It is therefore suggested that ca. 194 Ma is an important onset timing of widespread anorogenic magmatism in SE China. We interpret the early Jurassic mafic–ultramafic intrusion and A-type granites to represent an anorogenic magmatism in response to an onset of asthenospheric mantle upwelling due to the break-up of a subducted flat-slab beneath the SE China continent.

1. Introduction

The Mesozoic geology of Southeastern (SE) China is characterized by widespread igneous rocks consisting predominantly of granites and rhyolites, and subordinate mafic intrusive and volcanic rocks. In addition to the sporadically-distributed Triassic (referred to as "Indosinian" in the Chinese literature) intrusions (Wang et al.,

* Corresponding author. Tel.: +86 851 5895037; fax: +86 851 5891664.
E-mail address: zhuweiguang@vip.gyig.ac.cn (W.-G. Zhu).

0024-4937/$ – see front matter © 2010 Elsevier B.V. All rights reserved.
doi:10.1016/j.lithos.2010.07.005

2005a; Li et al., 2006), the late Mesozoic ("Yanshanian") igneous rocks fall into two main age groups: the Jurassic ("Early Yanshanian") and the Cretaceous ("Late Yanshanian") (e.g., Li, 2000; Zhou and Li, 2000; Zhou et al., 2006a; Li et al., 2007a) (Fig. 1). However, the protrogenesis of the Yanshanian magmatism and its tectonic implications has been a matter of extensive debate. Two major competing models exist, i.e., the subduction-related model (e.g., Jahn et al., 1976; Holloway, 1982; Jahn et al., 1990; Charvet et al., 1994; Martin et al., 1994; Lan et al., 1996; Lapierre et al., 1997; Sewell and Campbell, 1997; Zhou and Li, 2000; Zhou et al., 2006a), and the extension- and/or rift-related model (e.g., Gilder et al., 1991; Li and McCulloch, 1998; Chen et al., 1999; Li, 2000; Li et al., 2003, 2004; Wang et al., 2004, 2005b). More recently, Li and Li (2007) proposed a flat-slab subduction and slab-foundering model to account for both the wide Indosinian orogen and the broad Mesozoic magmatic province.

Based on compilation of published isotopic data (Zhou et al., 2006a), there appears to have been a magmatic quiescence during the early Jurassic (205–180 Ma) in SE China. Conversely, recent studies indicate that the early Yanshanian igneous rock in SE China might have initiated ca. 190 Ma (Ding et al., 2006; Li et al., 2007b; Yu et al., 2009). Thus, the onset time of the early Yanshanian magmatism in SE China is still controversial.

A number of Jurassic (178–165 Ma) A-type granites and alkaline syenites exist within the E–W trending Nanling Range from southern Jiangxi to southwestern Fujian province (Chen et al., 1998; Kong et al., 2000; Chen et al., 2002c; Li et al., 2003; Chen et al., 2005). Some mafic–ultramafic intrusions are associated spatially with these A-type granites in northeastern Guangdong and southern Jiangxi provinces, including the Xialan (~11.8 km^2), Yonghe (~18.8 km^2), and Changan (~8 km^2) intrusions (Xing et al., 2001; Chen et al., 2002a,b; Sun et al., 2002; Li et al., 2003; Yu et al., 2009). Studies on these mafic–ultramafic intrusions are important in understanding the role of mantle-derived magmas in the origin of the early Yanshanian magmatism and tectonic evolution of SE China. However, several studies have focused on the petrogenesis of the Xialan mafic–ultramafic intrusion, showing very different ages and Nd isotopic compositions (Xing et al., 2001; Yu et al., 2009). Yu et al. (2009) suggested that the Xialan intrusion was slightly younger than the Wengong granitic pluton in the Xingning area of NE Guangdong province, which is contrary to the field relationship. Thus, systematically geochronological, elemental and Nd–Sr isotopic investigations on the rocks are required to elucidate the genetic relationship between the Xialan and Wengong intrusions.

In this study, comprehensive analyses of precise SHRIMP and SIMS U–Pb zircon ages, geochemistry and Nd–Sr isotopes have been conducted on the Fe–Ti–V oxide ore-bearing Xialan mafic–ultramafic intrusion and the adjacent Wengong granites. The aims are to (1) determine the crystallization age for the mafic–ultramafic intrusion and spatially associated granitic pluton, (2) constrain the genetic link between the mafic–ultramafic rocks and the granites, and (3) shed new lights on the regional Jurassic magmatic–tectonic evolution.

2. Geological background and petrography

The Mesozoic granitoids and volcanic rocks are widespread in the southeast part of the South China block (Fig. 1; Zhou et al., 2006a; Li et al., 2007a). Among them, the early Yanshanian (ca. 190–150 Ma) granitoids are distributed mainly in the hinterland along the EW-trending Nanling Range and the NE-trending Wuyishan Mountains and in adjacent regions (Fig. 1), with a total exposed area of ca. 75,000 km^2 (Zhou et al., 2006a).

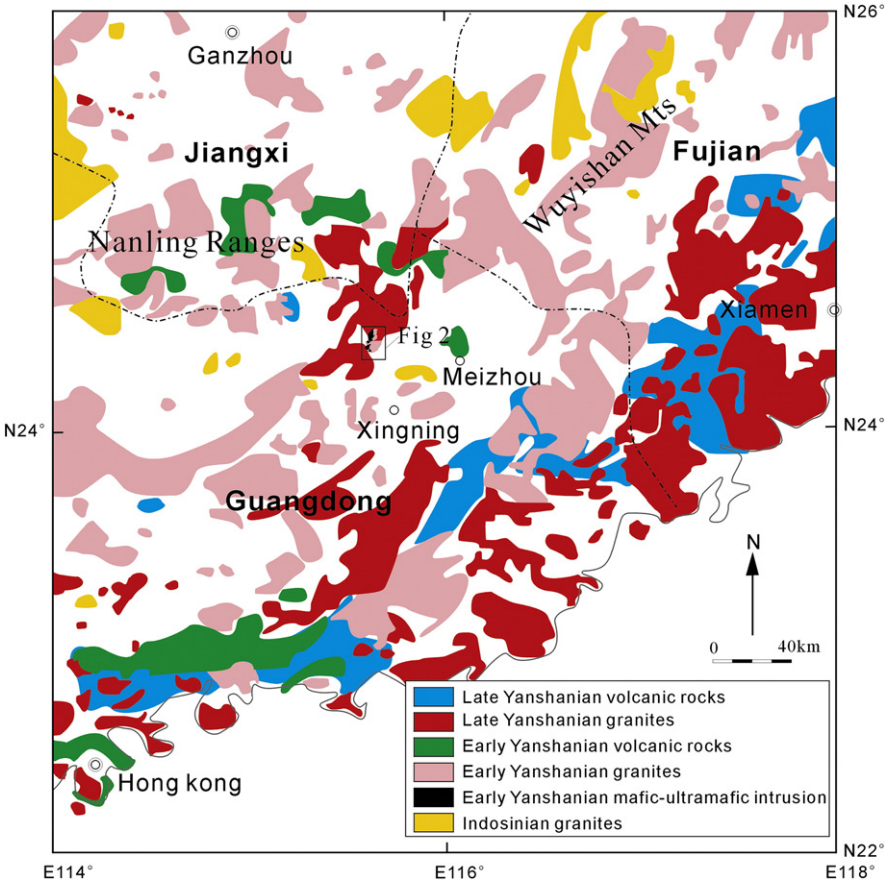

Fig. 1. Distribution of the Mesozoic igneous rocks in northeastern Guangdong, southern Jiangxi and southwestern Fujian region, southeastern China (modified after Zhou et al., 2006a; Li et al., 2007a).

The early Yanshanian A-type granites and alkaline syenites are generally adjacent to the bimodal volcanic rocks in the eastern section of the Nanling region, such as in southern Jiangxi, southern Hunan and southwestern Fujian, with some also in northeastern Guangdong (Chen et al., 1999, 2002c; Zhou et al., 2005, 2006b). The early Yanshanian alkaline and tholeiitic basalts also occur in southern and southeastern Hunan province (Chen et al., 1999, 2002c; Wang et al., 2004, 2005b; Zhou et al., 2006b). In addition, the early Yanshanian mafic dykes are sporadically distributed in southern Hunan and northern Guangdong (Wang et al., 2003; Li et al., 2004). The contemporaneous mafic–ultramafic intrusions have merely been reported, including the Xialan pluton in the Xingning area of northeastern Guangdong province and the Chebu pluton in southern Jiangxi province (Xing et al., 2001; Chen et al., 2002a,b; Sun et al., 2002; Li et al., 2003).

The Xingning area is located in a joint area between the eastern Nanling Range and the southwestern Wuyishan Mountains (Fig. 1). The basement rocks of the Cathaysia Block are composed mainly of the Paleoproterozoic high-grade metasedimentary Mayuan/Badu complex (Jin and Sun, 1997; Li, 1997; Li et al., 2000), late Mesoproterozoic igneous rocks (Chen et al., 2001; Xie et al., 2001) to earliest Neoproterozoic upper-greenschist to lower-amphibolite-facies metasedimentary rocks interbedded with felsic and mafic metavolcanic rocks of the Mamanshan and Longquan Groups (Li et al., 1999, 2005). However, there are as yet no reliable metamorphic ages reported for the Paleoproterozoic high-grade metasedimentary rocks. The basement rocks in the Xingning area are the late Neoproterozoic to early Palaeozoic metasedimentary rocks of the Yunkai Group (Wan et al., 2010), consisting of metamorphosed clastic rocks, gneisses and phyllites, as well as coeval monzogranites. The Ordovician and Silurian strata are missing in this area. The Devonian to early Carboniferous strata predominantly comprise clastic rocks, whereas the middle to late Carboniferous strata consist mainly of carbonate rocks. The Permian strata are composed of carbonate and clastic rocks. The early Triassic strata consist of mudstones and fine-grained clastic rocks, whereas the late Triassic strata are missing due to uplift and/or erosion. The Jurassic strata are characterized by mafic to felsic volcanic rocks interbedded with fine-grained clastic rocks. The Cretaceous strata comprise red-bed sediments (Chen et al., 2001; Sun et al., 2002).

Mesozoic magmatic rocks are widely distributed in the Xingning area, including granites, mafic–ultramafic intrusions, and their volcanic counterparts (Fig. 2; Xing et al., 2001, 2002; Chen et al., 2002a,b; Sun et al., 2002; Yu et al., 2009). The Xialan mafic–ultramafic intrusion was previously dated at 179 ± 4 Ma (Xing et al., 2001) and 195 ± 1 Ma (Yu et al., 2009) by Rb–Sr isochron and SHRIMP zircon U–Pb methods, respectively. The granite and mafic–ultramafic rocks intruded metasedimentary rocks of the Yunkai Group and the Carboniferous to Late Triassic strata (Xing et al., 2001), with hornfels, marbles and skarns observed in the contact zones. The adjacent Wengong granite separates the Xialan intrusion into northern and southern parts, with outcrops of ~8 km^2 and ~3.8 km^2, respectively (Fig. 2). The northern part of the Xialan intrusion is an elliptical body which is in fault contact with the Yunkai Group to the west (Fig. 2). It consists of three lithological zones: coarse- to medium-grained olivine gabbro and gabbro in the core, medium-grained gabbro in the transitional zone, and diorite in the margin (Fig. 2). The southern part of the Xialan intrusion is a 3.0 km-long, 1.2 km-wide and ~700 m-thick sill which dips 40–73° to northeast. It exhibits well-developed igneous layering and has been divided into three lithological zones from the bottom to top. Zone I in the lower part is composed mainly of coarse- to medium-grained gabbro and quartz-bearing gabbro, with minor plagioclase-bearing clinopyroxene peridotite and olivine gabbro. Zone II in the middle part is dominated by medium-grained gabbro and quartz-bearing gabbro with subordinate olivine-bearing gabbro. Zone III in the upper part is composed of clinopyroxene-bearing fine-grained diorite (Fig. 2). Plagioclase-bearing clinopyroxene peridotites comprise 50–80% olivine, 20–25% clinopyroxene and ≤5–30% plagioclase. Olivine gabbros consist of 25–40% clinopyroxene, 50–55% plagioclase, 10–20% olivine and minor hornblende (≤5%). Coarse- to medium-grained quartz diorites are composed of ~40% plagioclase, ~20% hornblende, ~10% quartz, 7–8% K-feldspar, and minor clinopyroxene and magnetite (Chen et al., 2002a). The present study focuses on coarse- to medium-grained gabbros from the Xianlan intrusion. The Xialan gabbros comprise 40–60% plagioclase, 30–50% clinopyroxene, 5–15% hornblende, and minor amounts of Fe–Ti oxides (magnetite and ilmenite) and quartz. Clinopyroxenes in the gabbros commonly exhibit coarse- to medium-grained texture. Electron microprobe analyses indicate clinopyroxenes from the gabbros are $Wo_{37-48}En_{28-47}Fs_{9-30}$, mostly belonging to augite (Appendix A). Hornblendes in the gabbros are generally observed at the rim of the clinopyroxene crystals. In addition, some fine-grained quartz-bearing diorites intruded in the margin of the Xialan intrusion. They are composed of 60–70% plagioclase, 15–20% hornblende, 7–10% clinopyroxene, 5–10% quartz, and minor biotite (≤5%). The disseminated V–Ti-magnetite ores occur mainly in the center of the northern part and Zone I and Zone II of the southern part of the Xialan mafic–ultramafic intrusion, composed of Ti–V-bearing magnetite and ilmenite (Chen et al., 2002a,b; Sun et al., 2002). The mafic–ultramafic intrusion contains over 200 million tons (Mt) of Fe–Ti–V oxide ores with an average grade of 17.34 wt.% FeO, 4.39 wt.% TiO_2, and 0.18 wt.% V_2O_5 (Wang, 1999).

The Wengong granite crops out over an area of 28 km^2 and intruded the Yunkai Group, the Xialan mafic–ultramafic intrusion, and the adjacent Jurassic volcanic rocks (Fig. 2). The pluton is composed of dominant coarse- to medium-grained hornblende K-feldspar granite in the center and subordinate medium- to fine-grained monzogranite in the marginal zone. The granite was classified as I-type granite and dated at 180 ± 1 Ma by the Rb–Sr isochron technique (Chen et al., 2002b). Rock-forming minerals include 30–60% K-feldspar, 25–40% quartz, 10–20% plagioclase, ≤5% hornblende, and minor magnetite, zircon and apatite.

3. Analytical methods

Zircon grains were separated from four gabbros and two granites using conventional heavy liquid and magnetic separation techniques. Representative zircon grains together with zircon standards (91500) were hand-picked under a binocular microscope and mounted in an epoxy resin disc, which was then polished to section the crystals in half for analysis. Zircons were documented with transmitted and reflected light micrographs as well as cathodoluminescence (CL) images to reveal their internal structures, and the mount was vacuum-coated with high-purity gold.

The U–Pb isotopic analyses for two samples (CQ0702 and LGXL-01) were performed using the Sensitive High-Resolution Ion Microprobe (SHRIMP II) at the Chinese Academy of Geological Sciences. Details of the analytical procedures for zircons using SHRIMP can be referred to Compston et al. (1992) and Song et al. (2002). Inter-element fractionation of ion emission of zircon was corrected relative to the standard zircon 91500 (Wiedenbeck et al., 1995). The uncertainties in ages are quoted at 1σ, and the pooled mean ages are quoted at 2σ or the 95% confidence interval. SHRIMP zircon U–Pb data for samples CQ0702 and LGXL-01 are presented in Appendix B.

Measurements of U, Th, and Pb for the other four samples (CQ0706, LGXL0701, WG0704, and WG0710) were conducted using the Cameca IMS-1280 ion microprobe at the Institute of Geology and Geophysics, Chinese Academy of Sciences, Beijing. U–Th–Pb ratios and absolute abundances were determined relative to the standard zircon 91500 (Wiedenbeck et al., 1995), analyses of which were interspersed with those of unknown grains, using operating and data processing procedures similar to those described by Li et al. (2009a). The mass resolution used to measure Pb/Pb and Pb/U isotopic ratios was 5400 during the analyses. A single electron multiplier was used in ion-counting mode to measure secondary ion beam intensities by peak jumping. Each measurement

consists of 7 cycles. Analyses of the standard zircon 91500 were interspersed with unknown grains. A long-term uncertainty of 1.5% (1 RSD) for $^{206}Pb/^{238}U$ measurements of the standard zircons was propagated to the unknowns (Li et al., 2010), despite that the measured $^{206}Pb/^{238}U$ error in a specific session is generally around 1% (1 RSD) or less. Measured compositions were corrected for common Pb using non-radiogenic ^{204}Pb. Corrections are sufficiently small to be insensitive to the choice of common Pb composition, and an average of present-day crustal composition (Stacey and Kramers, 1975) is used for the common Pb assuming that the common Pb is largely surface contamination introduced during sample preparation. Cameca SIMS zircon U–Pb dating results for these four samples are presented in Appendix C.

Chemical compositions of clinopyroxenes from the Xianlan intrusion were determined by wavelength-dispersion X-ray emission spectrometry using an EPMA-1600 electron microprobe at the State Key Laboratory of Ore Deposit Geochemistry (SKLOG), Institute of Geochemistry, Chinese Academy of Sciences (IGCAS). Major elements were obtained by PANalytical Axios-advance X-ray fluorescence spectrometer (XRF) at

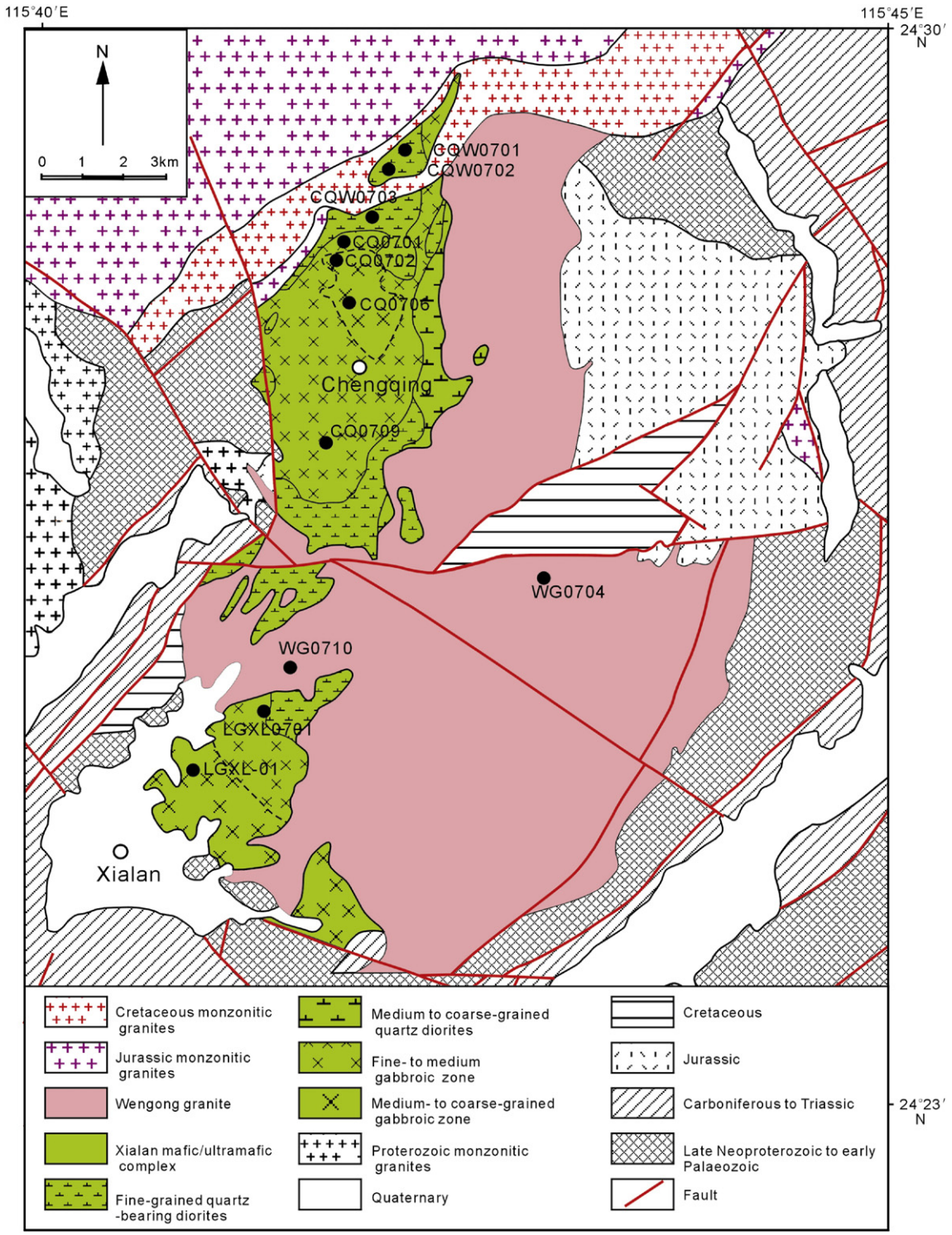

Fig. 2. Simplified geological map of the Xialan mafic–ultramafic intrusion and Wengong granitic pluton in the Xingning area, NE Guangdong province, showing the distribution of mafic–ultramafic bodies, diorites and granites (modified after IGGS, 2002).

the SKLOG, using fused lithum–tetraborate glass pellets. Analytical precision as determined on the Chinese National standard GSR-1 and GSR-3 were generally around 1–5%. Trace elements were analyzed by a Perkin–Elmer ELAN-DRC-e inductively-coupled plasma mass spectrometry (ICP-MS) at the SKLOG. The powdered samples (50 mg) were dissolved in high-pressure Teflon bombs using $HF+HNO_3$ mixture for 48 h at ~195 °C (Qi et al., 2000). Rh was used as an internal standard to monitor signal drift during counting. The international standards GBPG-1, OU-6, and the Chinese National standard GSR-1 were used for analytical quality control. The analytical precision is generally better than 5% for trace elements.

Samples for Nd–Sr isotopic measurements were spiked and dissolved in Teflon bombs with $HF+HNO_3$ acid, and separated by conventional cation-exchange techniques. The isotopic measurements were performed on a Finnigan MAT 262 multi-collector mass spectrometer at the Laboratory for Radiogenic Isotope Geochemistry, Institute of Geology and Geophysics, CAS. The measured $^{87}Sr/^{86}Sr$ and $^{143}Nd/^{144}Nd$ ratios are normalized to $^{86}Sr/^{88}Sr=0.1194$ and $^{146}Nd/^{144}Nd=0.7219$, respectively. The $^{87}Sr/^{86}Sr$ ratios of the NBS987 and NBS607 Sr standards and the $^{143}Nd/^{144}Nd$ ratios of the BCR-1 and La Jolla Nd standard solution determined during this study were 0.710265 ± 10 (2σ), 1.200468 ± 17 (2σ), 0.512624 ± 11 (2σ), and 0.511852 ± 6 (2σ), respectively.

4. Results

4.1. U–Pb zircon geochronology

4.1.1. Sample CQ0702 (gabbro from northern Xialan: N 24°28′28.9″, E 115°41′24.3″)

Zircons in sample CQ0702 are mostly euhedral, up to 100–150 μm long, and have length to width ratios of between 1:1 and 2:1. Most are

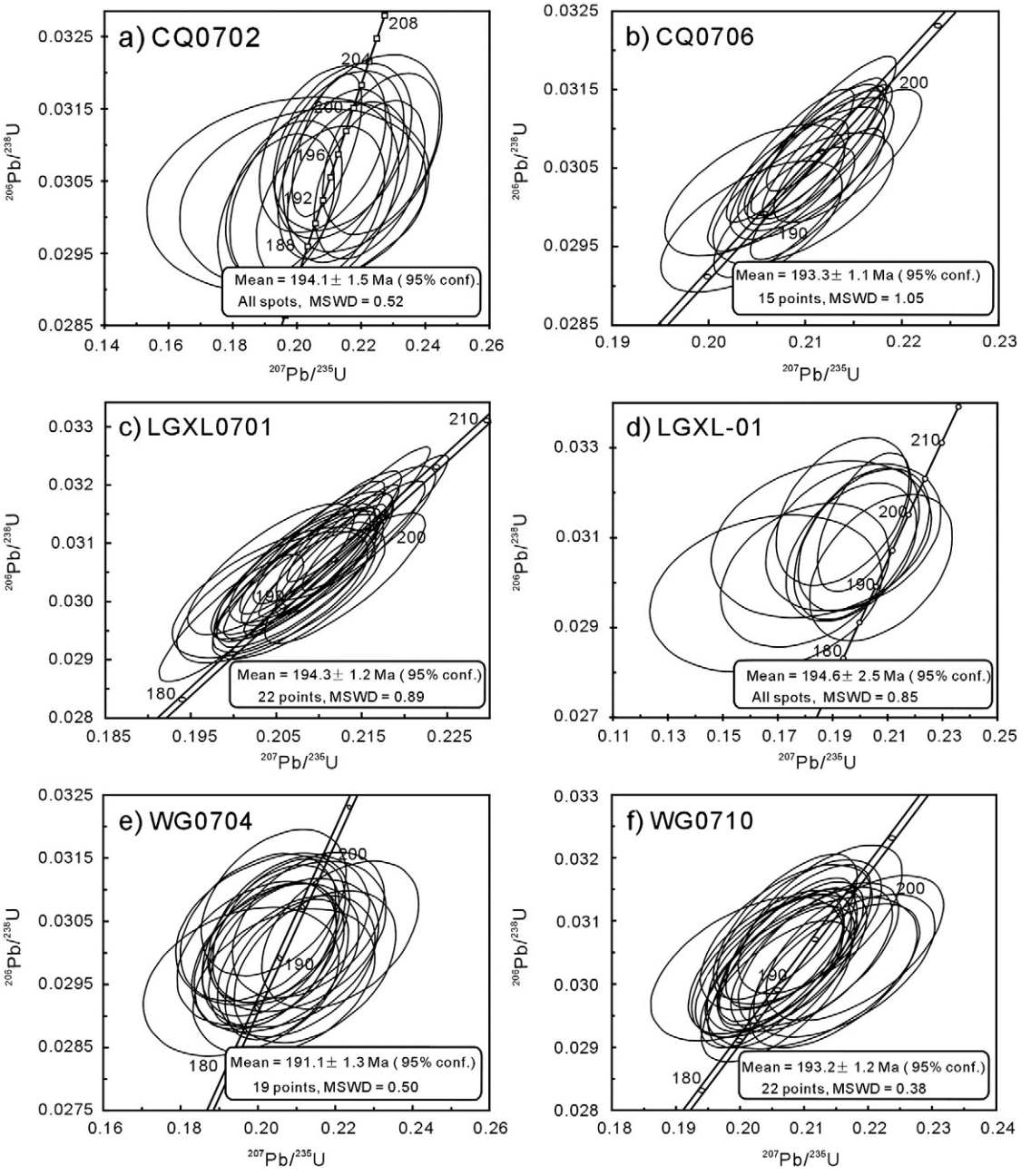

Fig. 3. SHRIMP and SIMS zircon U–Pb concordia diagrams for (a) sample CQ0702, (b) sample CQ0706, (c) sample LGXL0701, (d) sample LGXL-01, (e) sample WG0704, and (f) sample WG0710 from gabbros of the Xialan mafic–ultramafic intrusion and granites of the Wengong pluton in the Xingning area.

Table 1
Major element (in wt.%) and trace-element (in ppm) data for the gabbros of the Xialan mafic–ultramafic intrusion and the granites of the Wengong granitic pluton.

Rock type	Ore-barren gabbro	Ore-barren gabbro	Ore-barren gabbro	Ore-barren gabbro	Ore-bearing gabbro	Ore-bearing gabbro	Ore-bearing gabbro	Ore-bearing gabbro	Ore-barren gabbro	Ore-barren gabbro	Ore-barren gabbro	Ore-barren gabbro	Ore-barren gabbro	Ore-barren gabbro	Ore-barren gabbro	Ore-barren gabbro
Sample no.	CQ0701	CQ0702	CQ0703	CQ0704	CQ0705	CQ0706	CQ0707	CQ0708	CQ0709	LGXL0701	LGXL0702	LGXL0703	LGXL0704	LGXL0705	LGXL0706	LGXL0707
SiO_2	48.44	50.87	47.61	45.96	43.67	43.89	43.15	42.96	52.71	46.89	46.52	49.30	46.76	49.36	46.85	46.57
TiO_2	2.06	2.33	2.10	1.17	3.88	3.42	5.32	5.08	1.48	1.22	1.24	1.40	1.08	1.72	1.41	1.22
Al_2O_3	13.73	14.41	14.04	16.52	13.12	13.94	14.27	14.75	14.80	16.39	16.46	16.10	16.93	15.32	17.15	16.59
Fe_2O_3	13.18	15.91	14.05	12.30	17.31	17.80	17.53	16.49	9.89	10.31	10.10	10.39	9.80	11.27	10.48	10.95
MnO	0.20	0.33	0.23	0.18	0.20	0.21	0.20	0.18	0.15	0.14	0.14	0.14	0.13	0.16	0.14	0.16
MgO	6.24	2.75	6.21	8.22	6.62	6.72	6.46	6.80	5.24	9.12	8.61	7.43	9.24	6.66	7.85	8.23
CaO	10.60	7.52	10.66	11.41	11.75	10.94	10.41	10.65	8.75	11.28	11.47	10.54	12.05	11.30	11.38	10.92
Na_2O	3.13	3.96	2.72	2.12	2.45	2.70	2.48	2.45	3.14	2.25	2.42	2.51	2.03	2.83	2.69	2.67
K_2O	0.86	0.84	0.86	0.27	0.27	0.26	0.26	0.24	0.69	0.35	0.61	0.74	0.23	0.65	0.31	0.44
P_2O_5	0.19	0.94	0.38	0.13	0.13	0.12	0.11	0.10	0.18	0.12	0.12	0.11	0.09	0.16	0.13	0.13
LOI	1.35	0.35	1.48	1.60	0.66	0.83	0.64	0.83	1.70	2.27	2.51	2.13	2.46	1.61	2.38	3.27
Total	99.98	100.21	100.34	99.87	100.05	100.83	100.83	100.52	98.74	100.33	100.20	100.79	100.80	101.04	100.77	101.14
$Mg^{\#}$	48.4	25.5	46.7	57.0	43.1	42.8	42.2	45.0	51.2	63.7	62.8	58.6	65.1	53.9	59.7	59.8
Sc	42.0	25.5	36.8	29.4	42.3	39.2	38.9	35.7	22.6	25.9	29.2	28.1	29.7	34.6	26.1	25.3
V	354	45.3	272	207	658	583	528	561	189	203	218	258	186	261	231	173
Cr	61.2	21.5	200	218	44.4	65.8	13.0	29.4	68.5	171	185	175	291	88.1	215	210
Co	45.8	16.2	37.8	48.8	59.9	61.5	56.6	62.8	32.9	49.8	48.9	43.5	49.5	41.3	44.5	48.5
Ni	44.0	9.70	76.6	101	75.1	84.5	10.8	20.6	56.3	136	107	99.8	131	52.0	103	123
Cu	59.3	23.9	72.2	76.3	95.9	65.7	58.8	40.1	44.4	81.8	76.9	69.3	104	116	74.3	79.0
Zn	117	163	118	71.9	110	108	107	92.6	77.2	68.4	67.2	73.1	72.5	79.2	69.1	74.5
Ga	18.5	22.7	17.5	16.4	20.3	20.1	19.2	18.9	16.7	16.6	17.1	18.4	14.9	19.6	17.7	17.0
Rb	40.5	31.2	47.7	11.8	6.43	5.73	6.32	6.02	24.0	9.75	23.5	21.3	6.21	19.6	8.58	15.1
Sr	267	373	304	265	280	321	327	312	216	253	279	262	243	257	277	287
Y	26.4	49.6	27.3	10.9	17.5	13.9	13.4	12.2	22.8	17.4	17.1	23.2	14.7	28.2	17.2	18.3
Zr	96.4	66.8	79.9	35.8	80.2	51.3	60.3	47.7	60.2	79.3	83.8	115	71.0	97.4	75.5	80.6
Nb	9.76	31.7	10.1	3.11	7.39	4.65	8.86	5.90	12.1	7.10	6.74	10.4	5.03	9.21	6.64	8.14
Cs	2.32	2.30	3.16	1.51	0.75	1.94	1.91	1.44	3.17	2.29	2.65	1.89	1.21	1.52	1.53	1.36
Ba	135	239	123	37.8	58.9	59.1	56.7	52.2	139	62.3	81.3	153	50.6	104	43.7	49.9
La	11.3	30.9	11.9	4.00	6.36	5.29	5.00	4.68	15.4	8.01	7.18	14.9	5.80	11.4	6.95	8.47
Ce	26.4	72.4	28.4	9.59	15.3	12.3	11.7	10.9	32.4	18.4	16.9	32.5	12.7	25.7	16.4	19.5
Pr	3.70	9.95	4.14	1.40	2.26	1.82	1.71	1.60	4.14	2.51	2.35	4.26	1.84	3.72	2.42	2.83
Nd	16.5	44.8	19.1	6.89	11.0	8.76	8.69	7.81	16.5	11.1	10.9	18.1	8.28	17.1	11.0	12.6
Sm	4.34	10.9	4.98	1.80	3.02	2.36	2.26	2.07	4.02	2.82	2.84	4.39	2.26	4.60	3.03	3.22
Eu	1.42	3.78	1.95	0.977	1.15	1.24	1.24	1.03	1.14	1.07	1.03	1.25	0.869	1.50	1.10	1.21
Gd	4.87	11.5	5.78	2.09	3.50	2.76	2.66	2.46	4.18	3.22	3.34	4.64	2.69	5.34	3.42	3.47
Tb	0.802	1.68	0.897	0.353	0.590	0.471	0.443	0.403	0.664	0.553	0.524	0.756	0.415	0.876	0.588	0.589
Dy	4.81	9.48	5.09	2.05	3.47	2.73	2.61	2.32	4.03	3.18	3.09	4.49	2.49	5.26	3.41	3.53
Ho	1.04	1.96	1.09	0.448	0.708	0.607	0.556	0.492	0.847	0.704	0.658	0.935	0.519	1.11	0.720	0.765
Er	2.71	4.83	2.74	1.15	1.79	1.43	1.42	1.26	2.21	1.74	1.80	2.41	1.32	2.91	1.87	1.97
Tm	0.394	0.632	0.377	0.152	0.253	0.190	0.186	0.165	0.333	0.240	0.239	0.326	0.191	0.419	0.247	0.263
Yb	2.35	3.78	2.18	0.925	1.55	1.21	1.17	1.05	2.02	1.57	1.53	2.19	1.10	2.42	1.62	1.72
Lu	0.313	0.541	0.286	0.146	0.207	0.172	0.169	0.148	0.275	0.225	0.208	0.294	0.163	0.344	0.232	0.238
Hf	2.35	1.91	2.07	0.929	2.08	1.37	1.61	1.28	1.77	2.04	2.19	3.06	1.57	2.73	1.96	2.04
Ta	0.620	1.93	0.651	0.241	0.508	0.337	0.749	0.502	0.894	0.471	0.472	0.676	0.301	0.651	0.428	0.539
Pb	3.39	9.74	3.11	1.08	1.95	1.57	0.987	1.66	4.66	1.43	1.70	2.33	1.38	1.35	0.815	0.892
Th	1.74	3.64	1.47	0.688	0.904	0.815	0.752	0.792	4.39	1.25	1.01	3.17	0.784	2.05	0.922	1.14
U	0.315	0.629	0.318	0.139	0.206	0.165	0.171	0.171	0.883	0.250	0.248	0.634	0.200	0.426	0.225	0.249
T_{Zr} (°C)																

$Mg^{\#} = 100*$molar MgO/(Mg + FeO), assuming $FeO_T = 0.9 \times Fe_2O_3$. Total iron as FeO_T. T_{Zr} is calculated from zircon saturation thermometry (Watson and Harrison, 1983). LOI = loss on ignition.

Table 1 (*continued*)

Rock type	Ore-barren gabbro	Ore-barren gabbro	Ore-barren gabbro	Ore-barren gabbro	Ore-barren gabbro	granite	granite	granite	granite	granite	granite	granite	granite	granite	granite	granite	granite
Sample no.	LGXL0708	LGXL0709	LGXL0710	LGXL0711	LGXL-01	WG0701	WG0702	WG0703	WG0704	WG0705	WG0706	WG0707	WG0708	WG0709	WG0710	WG0711	WG0712
SiO_2	48.61	46.84	48.86	47.49	46.97	76.80	77.51	75.56	73.64	74.26	73.30	73.47	73.13	73.10	76.47	75.50	75.20
TiO_2	1.36	1.53	1.10	1.44	1.22	0.10	0.10	0.09	0.42	0.42	0.41	0.43	0.41	0.44	0.16	0.17	0.17
Al_2O_3	16.04	16.30	14.37	15.73	15.64	12.17	12.35	11.95	12.75	12.51	12.56	12.60	12.34	12.43	12.06	12.31	12.29
Fe_2O_3	10.14	10.83	9.22	10.48	9.54	1.30	1.50	1.25	2.73	3.14	3.36	4.08	3.21	3.46	1.80	1.90	2.00
MnO	0.15	0.15	0.14	0.14	0.13	0.01	0.00	0.01	0.06	0.06	0.09	0.13	0.08	0.06	0.01	0.03	0.03
MgO	7.09	7.95	9.31	7.53	9.02	0.10	0.10	0.12	0.22	0.27	0.24	0.26	0.23	0.41	0.11	0.17	0.15
CaO	11.36	11.28	12.64	10.95	11.52	0.43	0.26	0.41	0.72	0.28	0.84	1.16	0.89	0.71	0.07	0.60	0.54
Na_2O	2.81	2.60	2.15	2.74	2.37	3.77	4.01	3.85	3.81	3.85	4.54	3.92	3.83	4.09	3.84	4.01	3.94
K_2O	0.64	0.54	0.45	0.88	0.70	4.65	4.47	4.40	4.15	4.32	4.18	4.10	4.19	3.80	4.45	4.25	4.53
P_2O_5	0.15	0.13	0.08	0.13	0.11	0.02	0.02	0.02	0.06	0.06	0.06	0.06	0.06	0.06	0.02	0.02	0.02
LOI	1.71	2.52	1.81	2.84	2.89	0.74	0.55	0.68	0.93	0.71	0.87	0.74	0.69	1.22	0.87	1.04	0.99
Total	100.05	100.66	100.13	100.35	100.11	100.08	100.86	98.33	99.48	99.87	100.45	100.95	99.05	99.78	99.86	100.00	99.86
$Mg^{\#}$	58.1	59.2	66.7	58.7	65.2												
Sc	30.3	28.1	23.9	31.1	30.9	8.58	6.78	7.95	11.7	12.8	13.6	13.3	12.3	13.0	6.95	5.91	5.62
V	220	246	199	249	211	1.88	2.94	2.24	2.12	6.19	6.12	5.65	4.89	2.21	3.33	7.08	6.23
Cr	316	163	688	287	306	16.2	8.87	3.19	4.72	2.82	9.60	6.14	5.07	13.8	4.57	13.75	3.47
Co	41.4	46.5	39.6	43.6	45.9	0.310	0.207	0.152	0.846	0.882	1.04	0.863	0.775	1.04	0.596	0.557	0.683
Ni	93.2	103	144	96.5	123	6.70	3.32	2.40	4.24	1.09	4.68	2.96	2.69	19.1	1.97	6.73	2.42
Cu	84.7	80.8	156	85.0	79.6	8.69	4.72	4.27	4.61	4.35	4.85	6.52	4.10	4.59	5.14	3.74	2.97
Zn	82.9	73.3	54.4	73.3	63.5	32.7	20.1	25.6	85.0	71.1	86.2	82.4	67.4	65.4	74.1	72.2	85.0
Ga	18.1	17.8	15.6	17.8	16.3	22.6	20.5	22.5	18.9	18.9	20.2	20.4	20.0	20.1	19.5	21.2	21.2
Rb	18.3	22.1	10.3	36.5	32.0	224	192	200	134	157	154	145	154	128	178	170	184
Sr	269	279	209	266	308	15.7	15.2	15.8	105	81.6	106	126	109	103	32.6	30.4	26.4
Y	22.9	19.2	18.9	21.9	17.9	77.7	54.5	73.1	50.6	50.8	57.6	59.7	56.7	56.3	54.1	76.9	74.3
Zr	67.5	82.0	75.3	92.3	91.7	205	197	191	409	458	486	458	435	449	353	344	371
Nb	8.44	7.49	5.71	8.02	7.33	40.7	42.5	39.7	34.3	33.6	36.3	36.1	35.1	35.6	38.3	39.5	38.8
Cs	1.54	2.43	1.99	2.24	4.26	3.51	3.10	2.98	1.26	1.45	1.47	1.51	1.64	1.15	1.40	1.68	2.05
Ba	92.1	68.2	100	103	88.1	119	115	121	683	701	705	738	724	655	508	494	540
La	10.8	7.87	8.62	8.97	7.86	40.9	42.8	43.0	51.8	50.0	56.2	55.5	54.6	52.9	52.0	71.7	65.3
Ce	24.1	19.1	20.3	20.9	18.3	86.8	85.7	89.8	107	102	117	117	112	110	115	145	131
Pr	3.34	2.70	2.80	3.01	2.65	10.1	10.1	10.7	12.5	12.0	13.6	13.7	13.4	12.8	12.4	17.1	15.3
Nd	14.9	12.6	12.8	13.8	11.9	39.1	39.2	40.5	49.2	46.0	51.9	54.9	51.7	51.5	48.0	66.0	61.5
Sm	3.87	3.20	3.34	3.56	3.12	9.27	8.58	9.75	9.99	9.26	10.8	11.3	10.5	10.7	9.86	14.0	13.1
Eu	1.34	1.17	1.05	1.22	1.05	0.344	0.298	0.368	2.12	1.99	2.21	2.28	2.20	2.32	1.11	1.26	1.29
Gd	4.38	3.71	3.82	3.85	3.34	9.79	8.65	9.50	9.74	8.92	10.5	10.9	10.5	10.5	9.53	11.9	11.5
Tb	0.719	0.623	0.644	0.670	0.583	1.70	1.43	1.65	1.48	1.35	1.53	1.65	1.56	1.56	1.48	2.21	2.15
Dy	4.03	3.60	3.79	3.99	3.37	11.7	9.27	11.2	8.87	8.34	9.65	10.0	9.77	9.55	9.69	13.6	13.3
Ho	0.896	0.791	0.809	0.873	0.702	2.50	1.89	2.33	1.76	1.71	1.94	2.05	1.97	1.90	1.91	2.79	2.82
Er	2.42	2.03	2.11	2.16	1.75	6.73	5.22	6.45	4.92	4.91	5.27	5.57	5.36	5.34	5.15	7.89	7.44
Tm	0.302	0.273	0.284	0.300	0.249	1.01	0.744	0.960	0.698	0.684	0.754	0.791	0.770	0.729	0.768	1.12	1.08
Yb	1.97	1.72	1.77	1.89	1.59	6.43	4.65	6.02	4.35	4.57	4.96	5.01	4.91	4.74	4.65	7.15	7.18
Lu	0.285	0.258	0.250	0.270	0.216	0.885	0.619	0.802	0.651	0.676	0.715	0.745	0.737	0.695	0.655	1.034	0.992
Hf	1.85	2.00	1.95	2.29	2.29	7.80	7.25	6.81	10.33	10.96	11.60	10.96	10.48	10.53	10.36	10.96	12.03
Ta	0.571	0.469	0.385	0.544	0.504	3.48	3.56	3.25	2.30	2.27	2.51	2.33	2.34	2.34	2.96	3.20	3.36
Pb	1.84	0.711	1.76	1.28	0.672	15.3	10.6	10.2	30.1	22.7	39.6	32.0	23.8	16.4	27.8	32.1	29.2
Th	1.54	1.05	1.12	1.20	1.24	24.6	23.4	23.6	18.1	18.7	19.6	19.1	19.0	18.0	21.1	25.8	25.0
U	0.358	0.249	0.299	0.258	0.256	3.58	3.89	3.30	2.98	2.81	2.96	3.17	3.05	2.58	3.54	4.14	4.21
T_{Zr} (°C)						859	857	851	933	948	942	939	935	941	920	911	919

Table 2
Sr and Nd isotopic data for the gabbros of the Xialan mafic–ultramafic intrusion and the granites of the Wengong pluton.

Sample No.	Rb (ppm)	Sr (ppm)	$^{87}Rb/^{86}Sr$	$^{87}Sr/^{86}Sr$ (2σ)	I_{Sr}	Sm (ppm)	Nd (ppm)	$^{147}Sm/^{144}Nd$	$^{143}Nd/^{144}Nd$ (2σ)	$^{143}Nd/^{144}Nd$ (i)	εNd (T)	T_{DM} (Ga)	T_{2DM} (Ga)
Xialan gabbros													
CQ0702	31.39	352.7	0.2576	0.705951 (11)	0.70524	12.19	49.77	0.1480	0.512718 (12)	0.5125293	2.8		
CQ0705	6.425	280.4	0.0663	0.705057 (9)	0.70487	3.185	11.31	0.1703	0.512872 (15)	0.5126549	5.2		
CQ0706	6.851	371.2	0.0534	0.704588 (11)	0.70444	2.811	9.821	0.1730	0.512769 (14)	0.5125481	3.1		
CQ0707						2.647	9.143	0.1750	0.512782 (13)	0.5125582	3.3		
CQ0708	8.169	290.9	0.0812	0.705128 (11)	0.70490	2.503	8.772	0.1725	0.512762 (13)	0.5125422	3.0		
CQ0709	24.51	322.2	0.2201	0.705189 (10)	0.70458	5.501	22.56	0.1474	0.512663 (13)	0.5124744	1.7		
LGXL0701	11.53	271.3	0.1230	0.704783 (10)	0.70444	3.481	13.33	0.1579	0.512871 (12)	0.5126699	5.5		
LGXL0703	22.70	254.4	0.2582	0.705128 (9)	0.70442	4.744	19.41	0.1478	0.512777 (12)	0.5125885	3.9		
LGXL0704	6.544	251.8	0.0752	0.704281 (11)	0.70407	2.798	10.33	0.1637	0.512897 (12)	0.5126881	5.9		
LGXL0707	17.43	283.0	0.1782	0.704688 (12)	0.70420	3.696	13.93	0.1604	0.512908 (15)	0.5127036	6.2		
LGXL0710	13.25	196.9	0.1948	0.705064 (10)	0.70453	3.593	13.29	0.1635	0.512815 (12)	0.5126064	4.3		
LGXL-01	32.89	302.1	0.3151	0.706863 (11)	0.70599	3.498	13.10	0.1614	0.512890 (11)	0.5126841	5.8		
Wengong granites													
WG0701						9.626	41.19	0.1413	0.512629 (11)	0.5124489	1.2	1.10	0.88
WG0702						10.50	45.81	0.1386	0.512617 (11)	0.5124401	1.0	1.08	0.89
WG0704	134.3	105.2	3.698	0.719045 (19)	0.70884	11.70	56.38	0.1254	0.512414 (11)	0.5122543	−2.6	1.27	1.19
WG0709	131.1	132.8	2.859	0.719023 (12)	0.71114	12.80	55.60	0.1392	0.512419 (12)	0.5122415	−2.8	1.49	1.21
WG0710	182.6	33.97	15.62	0.747626 (24)	0.70454	11.61	54.48	0.1288	0.512529 (11)	0.5123646	−0.44	1.11	1.01
WG0712	167.0	26.2	18.54	0.759292 (9)	0.70816	12.94	60.98	0.1283	0.512536 (11)	0.5123724	−0.28	1.09	1.00

Chondrite uniform reservoir (CHUR) values ($^{87}Rb/^{86}Sr = 0.0847$, $^{87}Sr/^{86}Sr = 0.7045$; $^{147}Sm/^{144}Nd = 0.1967$, $^{143}Nd/^{144}Nd = 0.512638$) are used for the calculation. $\lambda_{Rb} = 1.42 \times 10^{-11}$ year^{-1} (Steiger and Jäger, 1977); $\lambda_{Sm} = 6.54 \times 10^{-12}$ year^{-1} (Lugmair and Harti, 1978). The I_{Sr}, $(^{143}Nd/^{144}Nd)_i$, ε_{Nd} (T) of the gabbros for the Xialan mafic–ultramafic intrusion and the granites for the Wengong pluton were calculated using age of 194 Ma. The details for single-(TDM) or two-stage model age (T_{2DM}) calculations are given by Jahn et al. (1999).

clear, prismatic grains with simple internal growth zoning. Fifteen SHRIMP analyses from this sample were conducted on 15 grains during a single analytical session. Measured U concentrations vary from 133 to 873 ppm, and Th range from 83 to 800 ppm, with Th/U ratios of 0.65–0.99 (Appendix B). The measured $^{206}Pb/^{238}U$ ages are in good agreement within analytical errors, and the mean yields an age of 194.1 ± 1.5 Ma (95% confidence interval) (Fig. 3a). This age is considered as the best estimate of the crystallization age for sample CQ0702.

4.1.2. Sample CQ0706 (gabbro from northern Xialan: N 24°28′15.5″, E 115°41′18.8″)

Zircon grains in sample CQ0706 are mostly euhedral, up to 50–100 μm in length, and have length to width ratios of between 1:1 and 2:1. Most are clear, simple prismatic crystals with magmatic oscillatory zonings under CL. Fifteen Cameca SIMS analyses were conducted on 15 zircons (Appendix C). Uranium and thorium concentrations are high but variable, with U = 441–2626 ppm, Th = 207–3496 ppm and Th/U = 0.40–1.33. All the analyses are concordant in U–Pb and Pb–Pb isotopes within analytical errors (Fig. 3b), and the weighted mean of $^{206}Pb/^{238}U$ yields an age of 193.3 ± 1.1 Ma (95% confidence interval). This age is interpreted as the best estimate of the crystallization age for sample CQ0706.

4.1.3. Sample LGXL0701 (gabbro from southern Xialan: N 24°25′42.8″, E 115°41′10.2″)

Zircons in sample LGXL0701 are mostly clear and euhedral, up to 50–100 μm long, and have length to width ratios of between 1:1 and 3:1. They show clear concentric zoning under CL, Twenty-two Cameca SIMS analyses give high and variable concentrations of U (441–2371 ppm) and Th (424–6428 ppm), with Th/U ratios of 0.96–2.71 (Appendix C). All the analyses give concordant U–Pb and Pb–Pb results within analytical errors (Fig. 3c). The weighted mean of $^{206}Pb/^{238}U$ gives an age of 194.3 ± 1.2 Ma (95% confidence interval), which is interpreted as the best estimate of the crystallization age for sample LGXL0701.

4.1.4. Sample LGXL-01 (gabbro from southern Xialan: N 24°24′58.7″, E 115°40′05.8″)

Zircon grains in this sample are mostly clear, euhedral prismatic grains with simple internal growth zonings under CL, up to 50–100 μm long, and have length to width ratios of between 1:1 and 3:1. U and Th contents vary from 129 to 1084 and 181 to 1817 ppm, respectively, with Th/U ratios of 1.13–4.66 (Appendix B). Twelve SHRIMP analyses were conducted on 12 zircons, and the measured $^{206}Pb/^{238}U$ ages agree internally to within analytical precision. The best estimate of the crystallization age of sample LGXL-01, based on the mean $^{206}Pb/^{238}U$ ratio, is 194.6 ± 2.5 Ma (95% confidence interval) (Fig. 3d).

4.1.5. Sample WG0704 (Wengong granite: N 24°26′30.8″, E 115°42′54.3″)

Zircons are mostly clear, euhedral prismatic grains with concentric zonings under CL, about 100 μm in length, and have a length to width ratio of between 1:1 and 1.5:1. Nineteen Cameca SIMS analyses were made on 19 zircons. These zircons have relatively low U (73–157 ppm) and Th (51–159 ppm) contents, with Th/U ratios varying between 0.63 and 1.01 (Appendix C). All the analyses are concordant in U–Pb and Pb–Pb isotopes within analytical errors (Fig. 3e). The weighted mean of $^{206}Pb/^{238}U$ corresponds to an age of 191.1 ± 1.3 Ma (95% confidence interval), which is the best estimate of the crystallization age of sample WG0704.

4.1.6. Sample WG0710 (Wengong granite: N 24°25′38.5″, E 115°41′24.3″)

Zircon grains in this sample are mostly clear and euhedral with concentric zonings under CL, ca. 100–200 μm long, and have a length to width ratio of between 1:1 and 2:1. Twenty-two analyses were conducted on 22 zircons. They show variable contents of U (160–505 ppm) and Th (107–449 ppm), with Th/U ratios of 0.61–1.07 (Appendix C). All the analyses give concordant U–Pb and Pb–Pb results within analytical errors (Fig. 3f). The weighted mean of $^{206}Pb/^{238}U$ yields an age of 193.2 ± 1.2 Ma (95% confidence interval), which is interpreted as the crystallization age of sample WG0710.

Combining the above dating results, the weighted mean of $^{206}Pb/^{238}U$ ages for the Xialan gabbros and the Wengong granites are 194 ± 1 Ma and 192 ± 1 Ma, respectively. The zircon U–Pb geochronology thus suggests that the studied gabbroic and granitic rocks formed almost synchronously within analytical uncertainties, although the field observations show that the Wengong granite intruded the Xialan mafic–ultramafic intrusion.

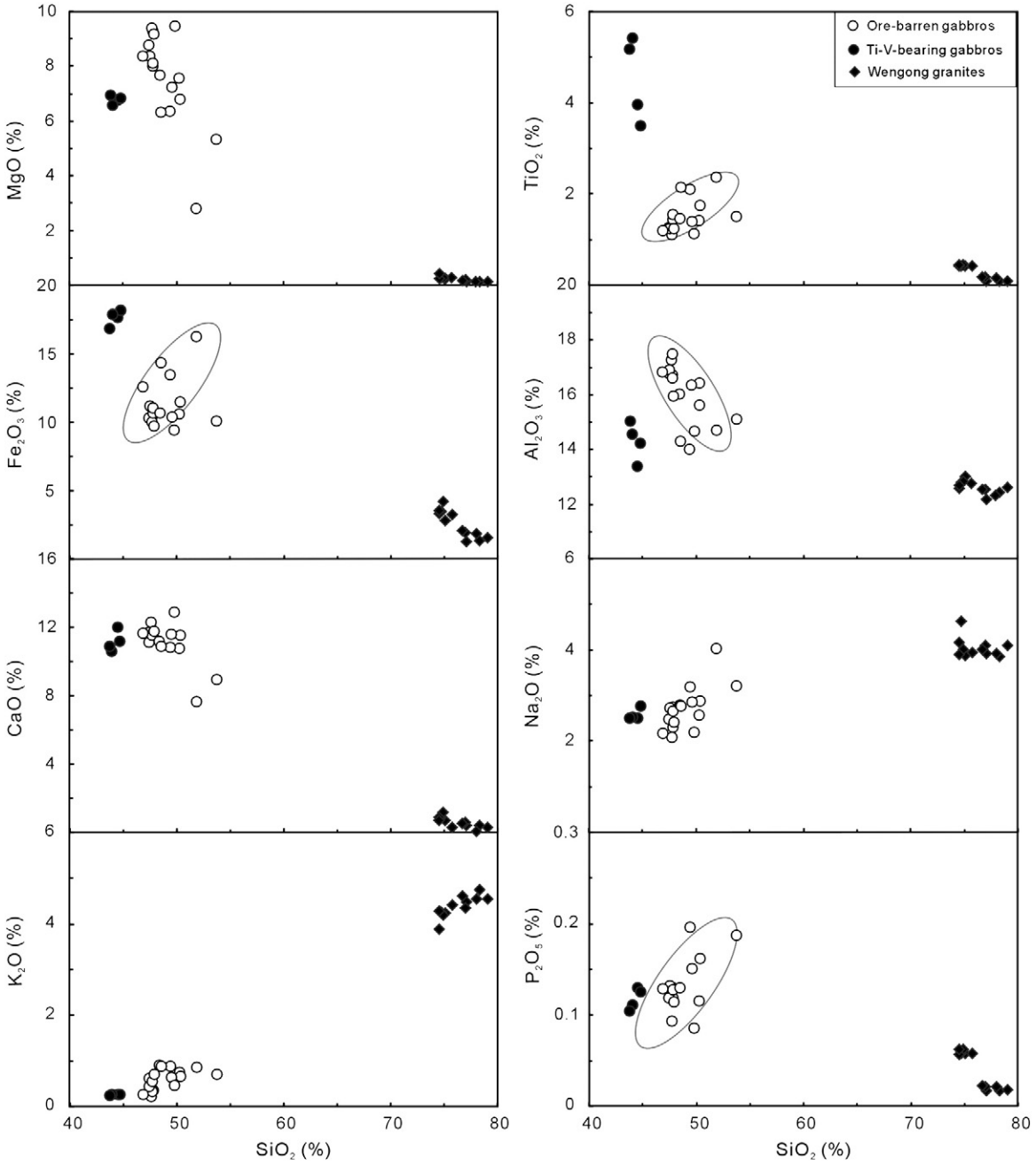

Fig. 4. Selected variation diagrams of major oxides and silica for gabbros from the Xialan mafic–ultramafic intrusion and granites from the Wengong granitic pluton.

4.2. Geochemical and Nd–Sr isotopic characteristics

Twenty-one gabbro samples from the Xialan mafic–mafic intrusion and twelve granite samples from the Wengong pluton have been selected for major and trace element analyses (Table 1). The major oxides described below are recalculated to 100% on a volatile-free base. Neodymium and Sr isotopes are determined for the representative samples from the Xianlan mafic–ultramafic intrusion and the Wengong granitic pluton (Table 2).

4.2.1. The gabbros of the Xialan intrusion

The ore-barren gabbros of the Xianlan intrusion display variably high Fe_2O_3 (9.4–16.2%, volatile-free), CaO (7.7–12.9%) and Al_2O_3 (14.0–17.5%) contents, with variable SiO_2 (46.9–53.8%), TiO_2 (1.1–2.4%), MgO (2.8–9.5%), total alkalis ($Na_2O + K_2O$ = 2.3–4.9%), and V (45–354 ppm) contents. In contrast, the Fe–Ti–V ore-bearing gabbros from the Xialan intrusion have higher Fe_2O_3 (16.8–18.2%), TiO_2 (3.5–5.4%) and V (528–658 ppm), and lower SiO_2 (43.8–44.8%) and ($Na_2O + K_2O$) (2.7–3.0%) concentrations than those of the ore-barren gabbros (Table 1). All the samples show evolved compositions with variable $Mg^{\#}$ number of 25.5–66.7. In the Harker diagrams (Fig. 4), MgO, CaO, and Al_2O_3 contents of the ore-barren gabbros decrease, whereas TiO_2, Fe_2O_3, Na_2O, K_2O, and P_2O_5 contents increase with increasing SiO_2 contents. The ore-barren samples have relatively high-Ti/Y ratios (287–657, mostly >400), similar to the high-Ti basaltic rocks (Peate et al., 1992; Xu et al., 2001). On the TAS rock classification diagram, these ore-barren rocks from the Xialan intrusion are plotted in the subalkaline field (Fig. 5). Moreover, they have relatively low Nb/Y ratios (0.29–0.66), an index of alkalinity, plotted exclusively into the subalkaline basalt field of the Nb/Y vs. Zr/TiO_2 diagram (not shown; Winchester and Floyd, 1976). Therefore, these rocks exhibit affinities with the high-Ti subalkaline basalts.

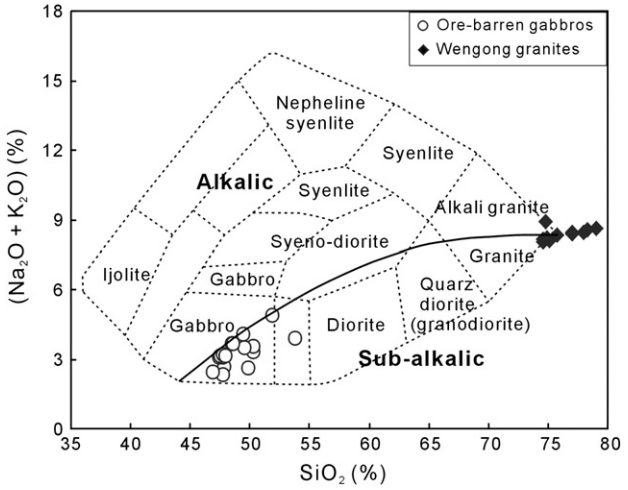

Fig. 5. Rock classification plots of SiO_2 vs. ($Na_2O + K_2O$) (Cox et al., 1979) for gabbros from the Xialan mafic-ultramafic intrusion and granites from the Wengong granitic pluton.

Despite variable REE abundances, the Xianlan gabbros display parallel REE patterns (REE = 32.0–207 ppm) with light rare earth element (LREE)-enriched and heavy REE (HREE)-depleted patterns (La_N = 13–100, $(La/Yb)_N$ = 2.8–5.5; Subscript N denotes the chondrite-normalized) (Boynton, 1984). Among them, the Fe–Ti–V ore-bearing gabbros have lower total REE contents with moderately positive Eu anomalies (Eu/Eu^* = 1.1–1.5) (Fig. 6a). In the primitive mantle-normalized spidergram (Sun and McDonough, 1989), all samples exhibit "convex upwards" patterns characterized by variable enrichment in incompatible elements between La and Th. The ore-barren rocks display weakly to insignificantly negative Nb–Ta anomalies relative to La (Nb/La = 0.66–1.03), but relatively high Th abundance, possibly due to crustal contamination. In contrast, the Fe–Ti–V ore-bearing samples exhibit obviously positive Ti and Sr anomalies due to variable degrees of accumulation of plagioclase and Fe–Ti oxides (Fig. 6b).

The Xialan gabbros have variable $^{147}Sm/^{144}Nd$ ratios between 0.1474 and 0.1750, and $^{143}Nd/^{144}Nd$ ratios between 0.512663 and 0.512908, corresponding to initial $\varepsilon_{Nd}(T)$ values between +1.7 and +6.2. These rocks also exhibit variable $^{87}Rb/^{86}Sr$ ratios between 0.0534 and 0.3151 and a relatively small range of $^{87}Sr/^{86}Sr$ ratios between 0.7043 and 0.7069, corresponding to initial I_{Sr} values between 0.7041 and 0.7060 (Table 2). The gabbros display positive $\varepsilon_{Nd}(T)$ and low I_{Sr} values, indicating that the magmas parental to the gabbros in the Xialan intrusion were derived from a depleted mantle source (Fig. 7).

4.2.2. The Wengong granites

The Wengong granites are highly siliceous and have a relatively small range of chemical compositions, with SiO_2 = 74.5–79.0% (volatile-free), Al_2O_3 = 12.2–13.0%, MgO = 0.10–0.42%, Fe_2O_3 = 1.3–4.2%, and CaO = 0.07–1.2%. Chemical analyses (Table 1) show that these rocks are rich in alkalis with K_2O (3.9–4.7%), Na_2O (3.8–4.6%), and total alkalis ($K_2O + Na_2O$ = 8.0–8.9%). Meanwhile, the granites

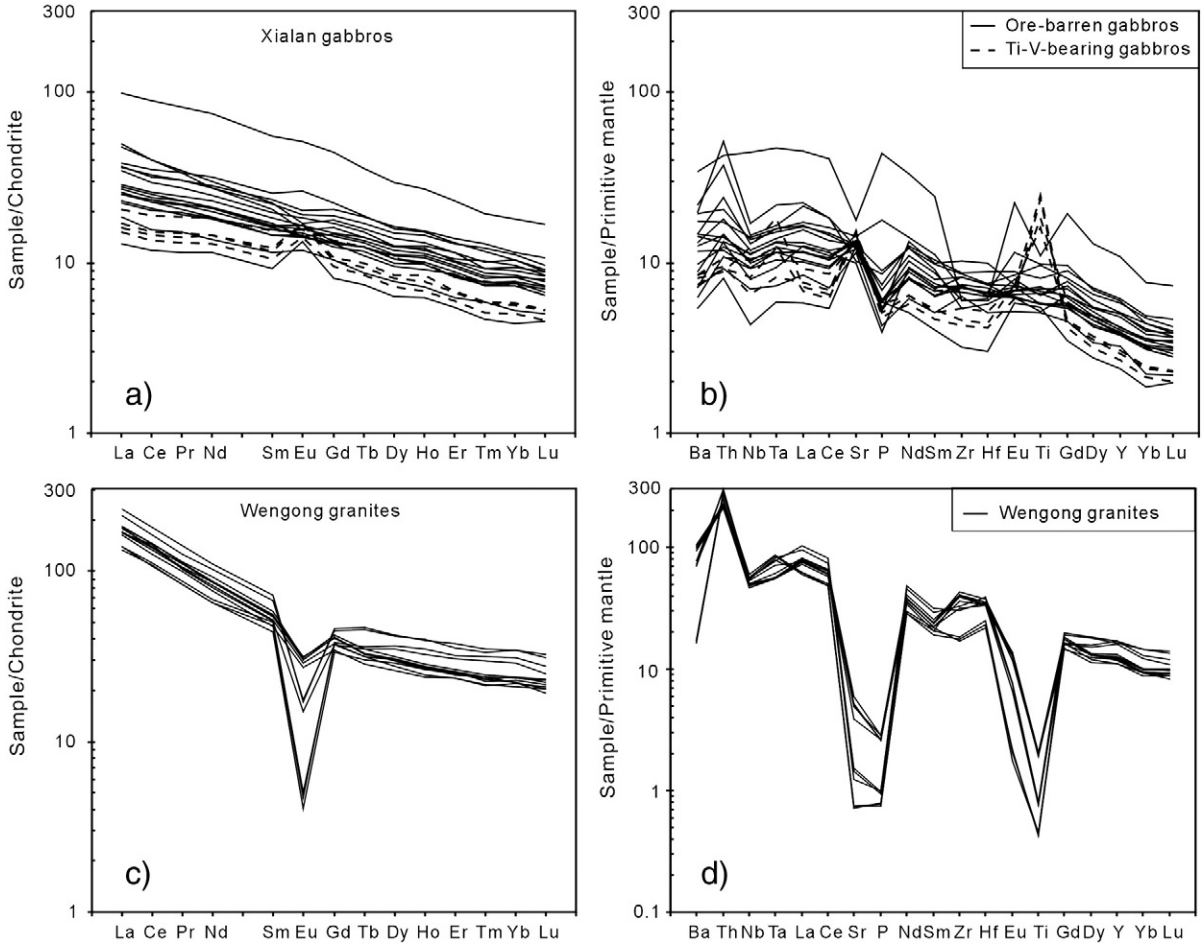

Fig. 6. Chondrite-normalized REE diagrams and primitive mantle-normalized incompatible trace-element spidergrams for gabbros of the Xialan mafic–ultramafic intrusion (a, b) and granites of the Wengong pluton (c, d). Chondrite-normalizing values are from Boynton (1984). Primitive mantle-normalizing values are from Sun and McDonough (1989).

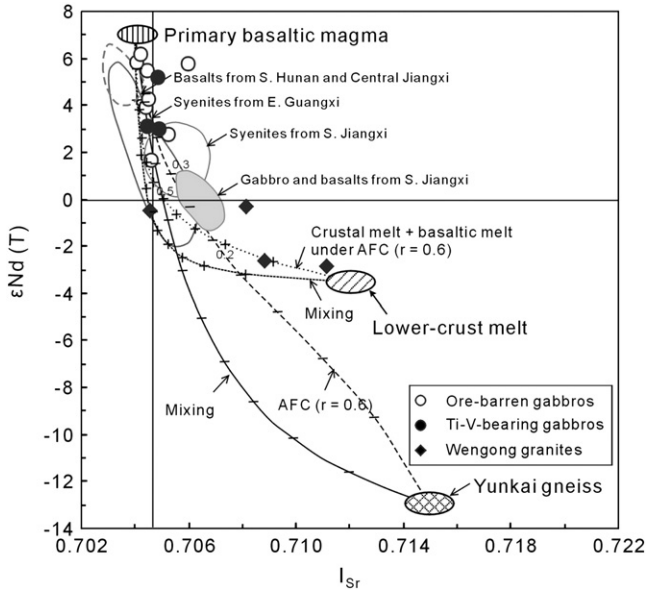

Fig. 7. Initial $\varepsilon_{Nd}(T)$ vs. I_{Sr} diagram for gabbros from the Xialan mafic–ultramafic intrusion and granites from the Wengong pluton. I_{Sr} ratios of the Wengong granites bear large uncertainties shown by error bars due to their relatively high Rb/Sr ratios. The data of basalts from southern Hunan and the central Jiangxi, syenites from eastern Guangxi, and gabbros and basalts from southern Jiangxi are from Li et al. (2007a). Numbers labeled on the AFC curves are the instantaneous mass fraction of the basaltic magma, and those labeled on the mixing curve are the fraction of the basaltic magma. The value of r is the rate of assimilation/rate of crystallization. The primary basaltic magma is assumed to have Sr = 375 ppm, Nd = 24.8, similar to the high-Ti and high-Fe basalt from Yongding of Fujian province (Zhou et al., 2006b), ε_{Nd} (194 Ma) = 7, and I_{Sr} (194 Ma) = 0.704. The contaminant crustal components (Sr = 107 ppm, Nd = 37.5, ε_{Nd} (194 Ma) = −13) are from the metasedimentary rock (gneiss) of the Yunkai Group in the Cathaysia Block (Wan et al., 2010), and I_{Sr} (194 Ma) = 0.715. The compositions of the lower-crust melt (Sr = 44.7 ppm, Nd = 95.8, ε_{Nd} (194 Ma) = −4) are the average of the rhyolitic rocks from the Mamianshan Group in the Cathaysia Block of southeastern South China (Li et al., 2005), and I_{Sr} (194 Ma) = 0.712. Because the chemical compositions of the Xialan intrusion are affinitive to high-TiO_2 basaltic melt, the partition coefficients between minerals and melt are used for the fractional crystallization: D^{Sr} = 0.7207 and D^{Nd} = 0.6382 [calculated for an assemblage with clinopyroxene, plagioclase, Fe–Ti oxide and olivine = 40/38/16/6 and D values in Rollinson (1993)]. The mixing and AFC trends (tick marks) are shown at 0.1 intervals.

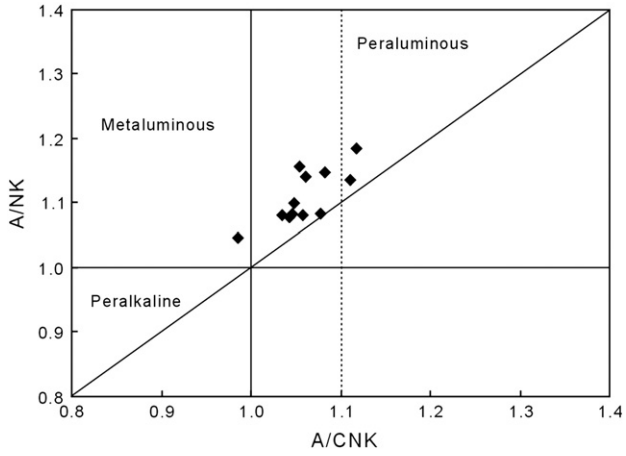

Fig. 8. A/NK vs. A/CNK plot showing the peraluminous nature of the Wengong granites. A/CNK = $Al_2O_3/(CaO + Na_2O + K_2O)$ molar, A/NK = $Al_2O3/(Na_2O + K_2O)$ molar.

belong to syenogranites and alkali granites in the R_1–R_2 classification diagram (not shown; De la Roche et al., 1980). As a result, the parental magmas of the Wengong granites exhibit affinity to a mildly alkaline magma. Their A/NK values range from 1.05 to 1.19, and A/CNK values from 0.98 to 1.12, falling into the weakly peraluminous area on the A/CNK vs. A/NK plot (Fig. 8). With increasing SiO_2 contents, contents of MgO, TiO_2, Fe_2O_3, Al_2O_3, CaO, and P_2O_5 decrease, whereas Na_2O contents remains nearly constant and K_2O slightly increases (Table 1; Fig. 4).

The Wengong granites show highly LREE-enriched (La_N = 132–231, $(La/Yb)_N$ = 4.3–8.0) and relatively flat-HREE ($(Gd/Yb)_N$ = 1.2–1.8) patterns, with significantly negative Eu anomalies (Eu/Eu^* = 0.11–0.67) (Fig. 6c). All the granitic rocks exhibit distinctly negative anomalies in Sr, P, and Ti in the primitive mantle-normalized spidergram (Sun and McDonough, 1989) (Fig. 6d). Meanwhile, these granitic rocks have variably high Ga (18.9–22.6 ppm), Rb (128–224 ppm), Zr (191–486 ppm), Nb (33.6–42.5 ppm), REE (219–363 ppm), and Y (50.6–77.7 ppm) concentrations, high FeO_T/MgO molar ratios (7.6–14.7) and total alkali contents, and relatively low Sr contents (15.2–126 ppm) (Table 1), exhibiting the characteristics of A-type granites (e.g., Collins et al., 1982; Whalen et al., 1987). The 10,000 × Ga/Al ratios of these granitic rocks range from 2.75 to 3.49, also similar to the global average of 3.75 for A-type granite (e.g., Collins et al., 1982; Whalen et al., 1987). In the diagram of Zr vs. Ga/Al (Fig. 9a), the Wengong granites are all classified as A-type granite. According to the geochemical subdivision of A-type granites by Eby (1992), the Wengong granites correspond to the A_2-type granites (Eby, 1992; Fig. 9b).

The Wengong granitic pluton displays slightly variable $^{147}Sm/^{144}Nd$ ratios ranging from 0.1254 to 0.1413, and the measured $^{143}Nd/^{144}Nd$ ratios are between 0.512414 and 0.512629, corresponding to initial $\varepsilon_{Nd}(T)$ values of −2.8 to +1.2 and two-stage Nd model ages (T_{2DM}) between 0.9 and 1.2 Ga (Table 2; Fig. 7). The four granitic samples have significantly variable $^{87}Rb/^{86}Sr$ (2.86–18.5) and $^{87}Sr/^{86}Sr$ (0.7190–0.7593) ratios, corresponding to the age-corrected I_{Sr} ratios ranging from 0.7045 to 0.7111. It is noted that the calculated I_{Sr} ratios for samples WG0710 and WG0712 (0.7045–0.7082) could bear large uncertainty due to their high Rb/Sr ratios (15.6–18.5).

5. Discussion

5.1. The petrogenesis of the Xialan gabbros

The Xialan ore-barren gabbros share similar evolutionary trends on the Harker diagrams (Fig. 4). Increase of TiO_2 and Fe_2O_3 with increasing SiO_2 indicates that TiO_2 and Fe_2O_3 were incompatible in the crystallizing phases and therefore titanomagnetite did not appear in the liquidus in the ore-barren rocks. The negative correlations of MgO, Fe_2O_3, CaO, and Al_2O_3 vs. SiO_2 imply that they may undergo some degrees of fractionation of plagioclase, olivine and/or clinopyroxene. However, the Fe–Ti–V ore-bearing gabbros have higher Fe_2O_3 and TiO_2 contents and significantly positive anomalies in Eu and Sr, suggesting that they are controlled dominantly by plagioclase and Fe–Ti oxides accumulation (Figs. 4 and 6a–b).

All the gabbros from the Xialan intrusion are slightly depleted in Nb and Ta (Fig. 6b), implying that a continental component must have been involved in their origin. However, these rocks have obviously higher $(Ta/La)_{PM}$ ratios than those of the subduction-related mafic rocks (Fig. 10a), suggesting their mantle source had not been affected by the ancient subduction-modified events (Hofmann and Jochum, 1996). Instead, the positive correlation between Nb/Th and Nb/La for the Xialan gabbros (Fig. 10b) suggests the involvement of Th-rich and Nb-depleted components in the magma. Furthermore, the $\varepsilon_{Nd}(T)$ values correlate negatively with La/Sm (Fig. 10c), indicating that the relative enrichment of La and depletion of Nb and Ta in the gabbros are mostly due to crustal contamination (e.g., Paces and Bell, 1989). These rocks showing high Th/U (3.8–5.8) ratios also support the suggestion that crustal assimilation will elevate Th/U ratios higher than MORB (~3.0) and OIB (~3.4) due to high Th/U ratios of crustal rocks (~5.0) (Rudnick and Fountain, 1995). Based on the above, a variable degree of wall-rock contamination may be the main factor causing low $\varepsilon_{Nd}(T)$, Nb/La and Nb/Th.

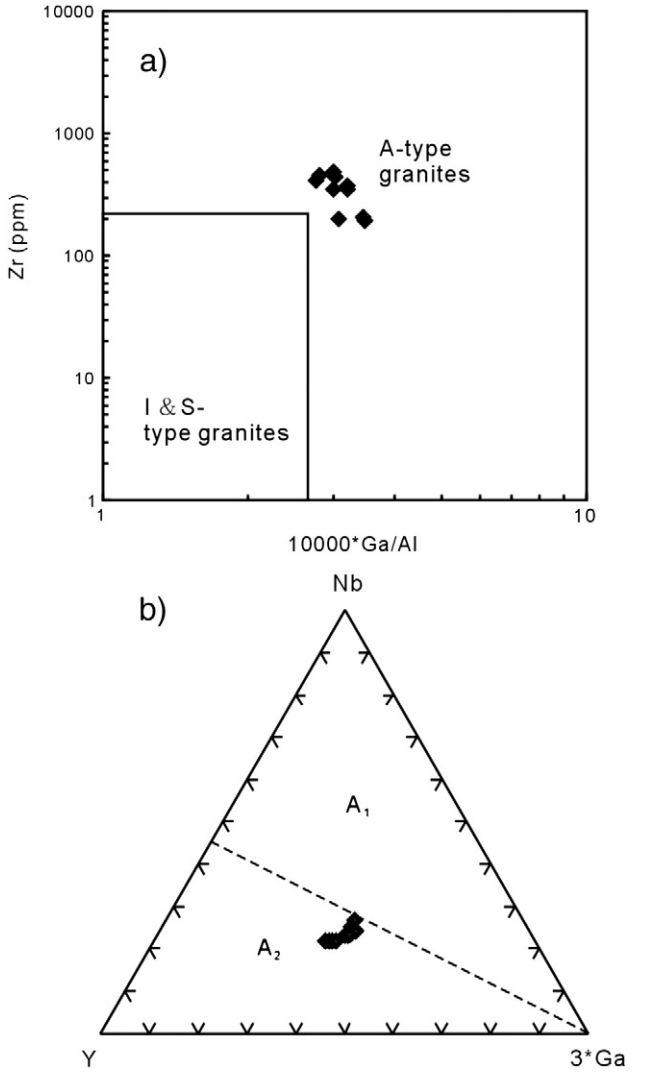

Fig. 9. Plots of (a) Zr vs. 10,000×Ga/Al and (b) Nb–Y–Ga ternary diagram for the subdivision of A_1- and A_2-type granites (Eby, 1992) showing the Wengong granites are affinitive to A_2-type granites.

We conducted quantitative modeling based on the Nd and Sr isotopic compositions by using the magma mixing and the assimilation and fractional crystallization (AFC) processes. We choose the high-Ti and high-Fe basalt from the Yongding area in Fujian province (Zhou et al., 2006b), with a compositional affinity to the Xialan gabbros (Xing et al., 2002), representing approximately the primary basaltic magma in this study. The compositions of the metasedimentary rock (gneiss) from the Yunkai Group are taken as the crustal contaminant (Wan et al., 2010). The calculation results are shown in Fig. 7. It appears that the binary mixing path is inconsistent with the variations in Nd and Sr isotopic compositions of the Xialan gabbros whereas the AFC path fits the compositional variations. The modeling results suggest variable amounts of crustal material (mostly 5–20%) were ingested into the primary melt parental to these gabbros.

Although the magmas parental to the Xialan gabbros were subjected to variable degrees of crustal contamination, the gabbros exhibit no significant Nb, Ta and Ti depletions relative to the neighboring elements (Fig. 6b), which are broadly similar to those of the intraplate basaltic rocks in CFB (continental flood basalt) and OIB (ocean island basalt) provinces (Sun and McDonough, 1989). Furthermore, the rocks have high-Ti/Y (mostly >400) and Zr/Ba (0.28–1.7), low La/Nb (0.56–1.5) and La/Ta (6.7–22), which is also similar to those of OIB (Ti/Y>410, Zr/Ba>0.2, La/Nb<1.5, and La/Ta<22) (Table 2; Ormerod et al., 1988; Sun and McDonough, 1989; Lightfoot et al., 1993; Garland et al., 1996; Ewart et al., 1998) and the adjacent early Yanshanian anorogenic extensional basalts in the Yongding area of NW Fujian province (Zhou et al., 2005, 2006b). In combination with their Nd isotopic features ($\varepsilon_{Nd}(T) = +1.7$ to $+6.2$), the parental magmas for the Xialan gabbros were generated dominantly by melting of a depleted asthenospheric mantle source.

5.2. The origin of the Wengong granites

The origin and petrogenesis of the A-type granites are quite controversial. Mechanisms involving melting of crustal and mantle sources, or fractional crystallization of basaltic magmas plus assimilation of crustal rocks, have been suggested (e.g., Collins et al., 1982; Whalen et al., 1987; Sylvester, 1989; Eby, 1992; King et al., 1997; Barbarin, 1999; Peccerillo et al., 2003). Therefore, the key issues

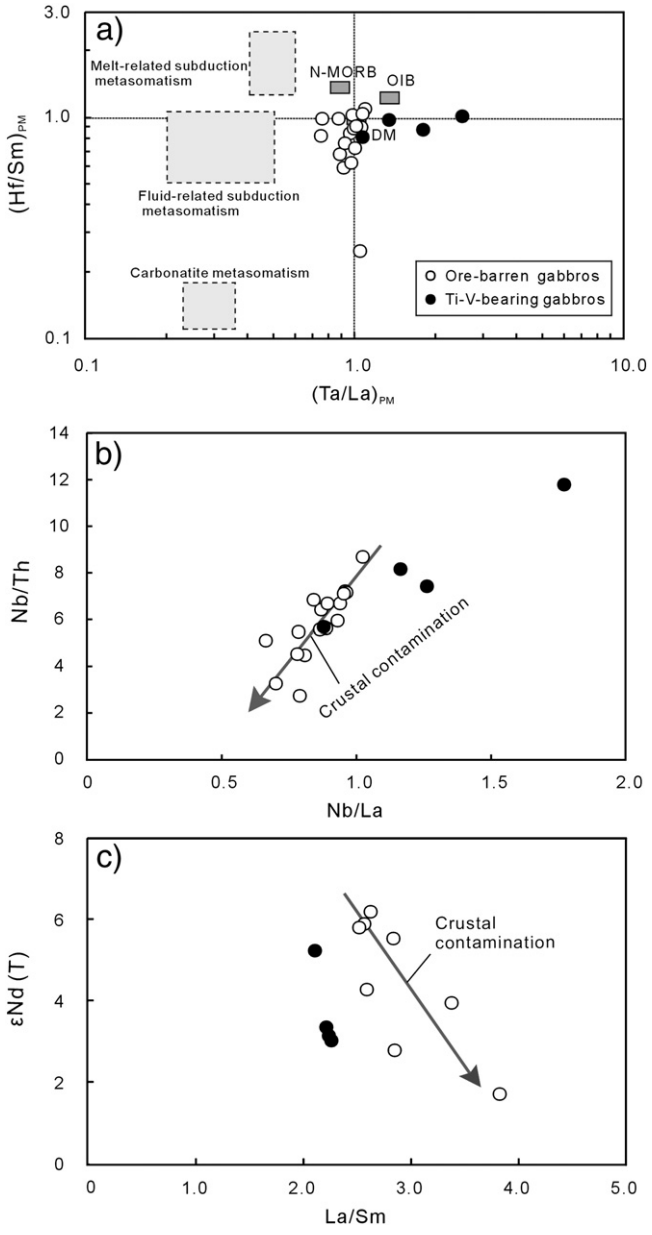

Fig. 10. Plots of (a) $(Hf/Sm)_{PM}$ vs. $(Ta/La)_{PM}$ (Hofmann and Jochum, 1996), (b) Nb/Th vs. Nb/La, and (c) $\varepsilon_{Nd}(T)$ vs. La/Sm for gabbros of the Xialan mafic–ultramafic intrusion. Subscript PM denotes the primitive mantle-normalized. Primitive mantle-normalizing values are from Sun and McDonough (1989).

concerning A-type granitoid origin are the role of mantle-derived material and its interaction with lower to middle continental crust.

The compositional variations of the Wengong granites imply various degrees of fractional crystallization (Fig. 4). The granites are characterized by very low MgO and Fe_2O_3 contents (Table 1 and Fig. 4), which is interpreted as due to the fractionation of MgO- and Fe_2O_3-rich minerals such as hornblende. From the REE patterns, hornblende may be considered as an important phase fractionated from magmas, because it is able to produce a fairly flat-HREE pattern without significant HREE fractionation in intermediate and acidic magmas (Martin et al., 1994; Han et al., 1997). The presence of Eu, Sr and Ba negative anomalies in the Wengong granites are hence indicative of fractionation of both plagioclase and K-feldspar (Figs. 6c–d and 11a) (Wu et al., 2002). The relative importance of plagioclase vs. alkali K-feldspar in a fractionation trend can be assessed using Eu/Eu* vs. Sr and Ba diagrams (Fig. 12a and b). It is therefore suggested that the evolution of the Wengong granites was controlled largely by plagioclase and minor alkali feldspar fractionation, consistent with the predominance of plagioclase in these rocks. A negative Ti anomaly is commonly related to ilmenite or titanite fractionation (Fig. 6d). In addition, P_2O_5 contents decrease with increasing SiO_2, showing apatite fractionation (Fig. 4). Several highly fractionated granitic samples (WG0701, WG0702, and WG0703) having relatively low REE contents were probably due to more apatite fractionation and consequent depletion of REE in the melt (Table 1; Watson and Capobianco, 1981). As a result, these chemical variations for the Wengong granites are consistent with the crystal fractionation of ferromagnesian minerals, plagioclase, Fe–Ti oxides and minor apatite.

Although the Wengong granites could have been produced by extreme differentiation of contemporaneous basic parental magma plus crustal contamination (e.g., Turner et al., 1992; Bonin, 1996), it is unlikely in this case for several reasons. Firstly, the Wengong granites show Nd–Sr isotopic compositions obviously different from the Xialan gabbros (Fig. 4). Secondly, there is a "Daly gap" between the mafic and felsic rocks. Thus, the magmas parental to the Wengong granites were unlikely a single fractionated melt from the basaltic magma generating the Xialan mafic–ultramafic intrusion.

As stated above, the Wengong granitic rocks are affinitive to A_2-type granites (Fig. 9b) based on the geochemical subdivision of A-type granites by Eby (1992). The A_2 group represents magmas derived from continental crust or underplated crust that have been through a cycle of continent–continent collision or island-arc magmatism (Eby, 1992). On the other hand, as suggested by many researchers, alkaline felsic magmas can also be generated by melting of basaltic rocks, leaving residues dominated by plagioclase and pyroxene (Thy et al., 1990; Beard and Lofgren, 1991; Hay and Wendlandt, 1995; Li et al., 2005). The whole-rock two-stage Nd model ages (T_{2DM}) of the Wengong granites range from 0.9 to 1.2 Ga (Table 2), implying that the Paleoproterozoic to late Neoproterozoic lower crust could be a potential source for the studied granites. Previous studies have shown that the Paleoproterozoic is an important time of crustal growth in SE China (Li et al., 2000). The regional Paleoproterozoic LREE-enriched-type amphibolites from the Cathaysia basement in SE China have initial ε_{Nd} values of 7.5–8.4 at 1766 Ma (Li et al., 2000), corresponding to ε_{Nd} values from −3.3 to −6.5 at 194 Ma. The recalculated Nd isotopic compositions are close to the minimal ε_{Nd} values (−2.8 to −2.6) of the Wengong granites. It has been suggested that these amphibolites had experienced amphibolite-facies metamorphism and extensive deformation (Jin and Sun, 1997; Li, 1997; Li et al., 2000), which could represent a part of the lower crust during the early Yanshanian stage. It is thus plausible to propose that the Wengong granitic pluton originated mainly from partial melting of the Paleoproterozoic lower crust in the Xining area.

However, the ε_{Nd} values of the Wengong granites vary between −2.8 and +1.2, indicating that the felsic magmas had mixed with variable amounts of upwelling basaltic magmas (Fig. 7). On the basis of Nd and Sr isotopic compositions, we conducted quantitative modeling to determine the incorporated amounts of the basaltic melt. Considering that the regional Mamianshan rhyolitic rocks formed at ca. 825 Ma could have been produced through partial melting of the Paleoproterozoic LREE-enriched-type amphibolites (Li et al., 2005), we choose the average compositions of the least-contaminated felsic volcanic rocks from the Mamianshan Group in the Cathaysia Block as an end-member of the lower-crust melt. The high-Ti and high-Fe basalt from Yongding of Fujian province (Zhou et al., 2006b) is used to approximate the basaltic magma. As shown in Fig. 7, the modeling result suggests that mixing of the crustal melt with various amounts of basaltic melt (5–45%) could produce melts with Nd and Sr isotopic compositions characteristic of the Wengong granitic rocks. As a result, the Wengong A-type granites were probably formed dominantly by the interaction between various amounts of crustal melt and mantle melt.

The Wengong granites exhibit continuously decreasing Zr with increasing SiO_2 (Fig. 11b), which are consistent with zircon separation from the evolving melt. Zircon saturation thermometry (Watson and Harrison, 1983) provides a simple and robust means of estimating magma temperatures from bulk-rock compositions. The calculated zircon saturation temperatures (T_{Zr}) of the Wengong granites are 851–948 °C (Table 1). Attaining the required high melting temperature (>900 °C) to generate siliceous A-type rocks at the lower crust requires extensive heat transfer from mantle-derived, hot basaltic magmas. As shown above, the emplacement age of the Wengong granites is slightly younger than the associated Xialan mafic–ultramafic intrusion. Therefore, the anorogenic basaltic magmas similar to those generating the Xialan gabbros might provide the heat source for partial melting of the lower-crust rocks. It has been suggested that bimodal intraplate magmatism could result from mantle upwelling (Hoffman, 1989). Li and Li (2007) proposed that the asthenospheric mantle upwelling might account for the early Jurassic anorogenic extensional magmatism in SE China. Moreover, the small amounts of melting (~20%) could generate felsic magmas by partial melting of amphibolitic lower crust under relatively low temperature

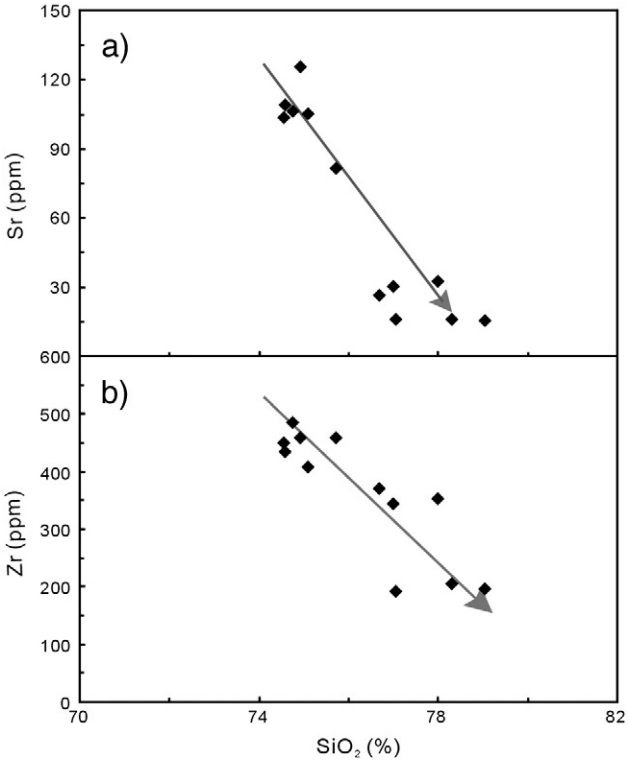

Fig. 11. Plots of (a) Sr vs. SiO_2, and (b) Zr vs. SiO_2 for the granites from the Wengong pluton.

(900–950 °C; Guffanti et al., 1996; Borg and Clynne, 1998). In the Xialan case, the basaltic magmas parental to the mafic–ultramafic intrusion erupted firstly to the upper-crustal magma chamber. Subsequently, relatively large amounts of basaltic magmas would be continuously underplated at or near the base of the crust induced by the asthenospheric mantle upwelling. The heat released from these magmas thus partially melted the fusible part of the lower crust and thereby generates the felsic melt. The basaltic magmas are likely to be trapped in the lower crust because the mafic melts cannot migrate through the less dense intermediate-silicic melt body (Huppert and Sparks, 1988; Riley, et al., 2001). The magmas were thereafter injected into the shallow-level chamber due to density contrast and gave rise to the Wengong granitic pluton.

As a result, we propose that the magmas parental to the Wengong granites are alkaline felsic melts, which were most probably generated by partial melting of the pre-existing Paleoproterozoic lower crust, and then mixed to varying degrees with the early Jurassic mantle-derived basaltic magmas. The resultant magmas would further experience extensive magmatic differentiation to account for the observed geochemical features of the Wengong granites.

5.3. Tectonic implications

The early Yanshanian magmatic rocks are widespread in the eastern and central parts of the Nanling granite belt of SE China. However, the tectonic regime accounting for these rocks has long been debated. Many previous studies favored an active continental margin related to subduction of the paleo-Pacific plate since early Jurassic for the Jurassic to Cretaceous magmatism in SE China (e.g., Jahn et al., 1990; Charvet et al., 1994; Martin et al., 1994; Lan et al., 1996; Lapierre et al., 1997; Sewell and Campbell, 1997). While this subduction-related model is feasible for the origin of the Cretaceous calc-alkaline magmatic belt in the coastal region, it fails to explain the exceptionally wide Jurassic magmatic province in the interior. To explain the formation of this wide Jurassic inland magmatic province, some modified subduction models were proposed. Zhou and Li (2000) suggested an increase of slab dip of the paleo-Pacific plate subduction underneath Southeast China from a very low angle in early Jurassic to a medium one in late Cretaceous time. Similarly, Jiang et al. (2009) proposed that these inland magmatic rocks were formed during the roll-back of the subducted slab. Alternatively, some others interpreted that the Jurassic inland magmatism was generated in response to the post-Indosinian orogenic extension (Chen et al., 2002c; 2008).

It is noted that all the aforementioned subduction models have difficulties to reconcile with the fact that most of the basaltic and alkaline rocks exhibit typical OIB geochemical characteristics (e.g., Li et al., 2003, 2004; Wang et al., 2004, 2005b; Li et al., 2007a,b, 2009b; Yu et al., 2009). Therefore, an alternative intracontinental extension or rifting model was proposed for the genesis of the Jurassic inland magmatism (Li et al., 2003, 2004; Wang et al., 2004). More recently, Li and Li (2007) used a flat-slab subduction/slab-foundering model to explain the ca. 1300-km-wide Indosinian Orogen in SE China. The early Yanshanian inland magmatic flare-up was interpreted as a response to the upwelling of asthenopheric mantle and basaltic underplating during the break-up and foundering of this flat-subducted oceanic lithosphere in early Jurassic (~190 Ma). This new model and the timing of the transition from the Indosinian orogenic to the early Yanshanian anorogenic magmatism, or initiation of the early Yanshanian magmatism, still awaits further investigation.

Our present study of the Xialan mafic–ultramafic intrusion and the Wengong granites sheds new lights on the tectonomagmatic evolution of SE China. The geochronological research demonstrated

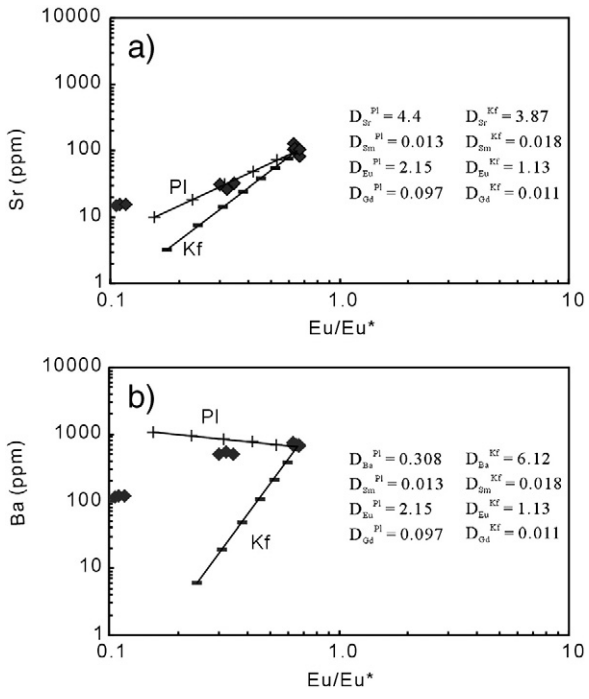

Fig. 12. Plots of (a) Eu/Eu* vs. Sr, and (b) Eu/Eu* vs. Ba for the granites from the Wengong pluton. Vectors for plagioclase (Pl) and K-feldspar (Kf) fractionation are calculated using partition coefficients of Arth (1976), indicating the importance of plagioclase fractionation and minor K-feldspar in the evolution of the granitic rocks. The composition of the granitic sample (WG0903) is assumed to represent the starting composition of the Wengong granites. Tick marks indicate percentage of mineral phase removed, in 10% intervals.

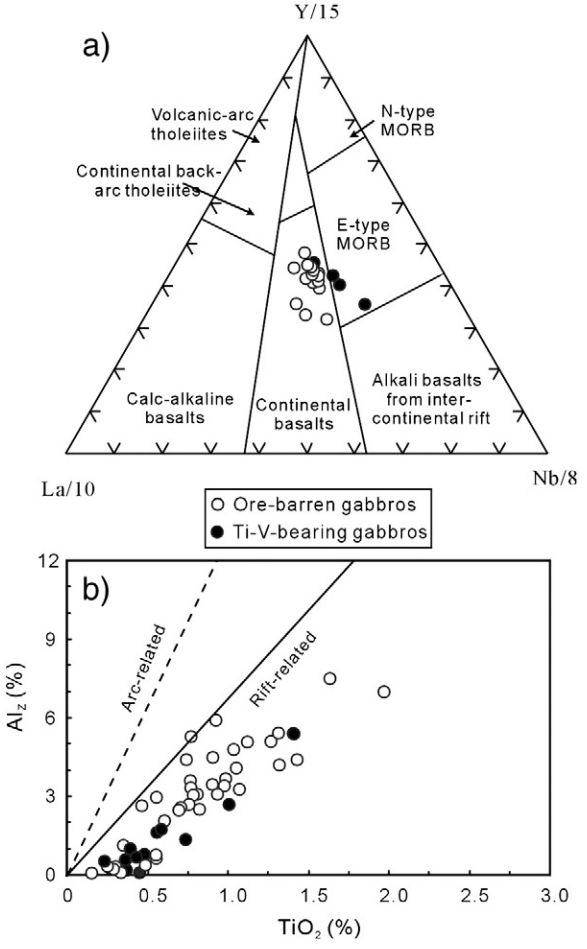

Fig. 13. Discrimination diagrams of (a) La/10–Y/15–Nb/8 (Cabanis and Lecolle, 1989), (b) Al_Z (percentage of tetrahedral sites occupied by Al) vs. TiO_2 in clinopyroxenes (Loucks, 1990) from the gabbros of the Xialan mafic–ultramafic intrusion.

here lead us to conclude that the emplacement of the Xialan mafic–ultramafic intrusion and the Wengong A-type granites took place in a short interval between 194 and 192 Ma. Although the Wengong granites are slightly younger than the Xialan gabbros, we consider that the granitic plutons formed coevally with or a few million years later than the mafic–ultramafic intrusion.

The Xialan gabbros exhibit a broadly geochemical similarity to the anorogenic extension-, rather than the subduction-related, basaltic rocks. On the La–Y–Nb discrimination diagram of Cabanis and Lecolle (1989), all the ore-barren Xialan gabbros fall into the continental basalt field (Fig. 13a). It is noteworthy that clinopyroxenes from the Xialan gabbros have high TiO_2 contents and quite low Al/Ti ratios (Fig. 13b; Loucks, 1990), typical of anorogenic extension-related mafic–ultramafic cumulative rocks. Therefore, the Xialan gabbros are likely formed in a continental anorogenic extensional environment.

A-type granites are generally formed in extensional environments (Whalen et al., 1987; Sylvester, 1989; Rogers and Greenberg, 1990; Eby, 1992; Nedelec et al., 1995; Barbarin, 1999; Frost et al., 2001), which might be related to different tectonic settings such as anorogenic rift, lithospheric extension, and late- to post-orogenic settings. Although the Wengong granites show affinities to A_2-type granites (Fig. 9a and b) that could have been generated in a late- to post-orogenic setting, they are temporally and spatially associated with the Xialan mafic–ultramafic intrusion. In addition, these granites are characteristically high in zircon saturation temperatures of up to 900 °C and HSFE abundances (Table 1). On the Nb vs. Y diagram, all the granites are plotted exclusively into the within-plate granite field (Fig. 14). The above features indicate that the Wengong A-type granites were more likely generated in an anorogenic extensional setting.

Our precise U–Pb zircon dating results demonstrate that the studied mafic and granitic rocks in the eastern Nanling Range were emplaced at ca. 194–192 Ma. These new isotopic dates argue against the previously proposed early Jurassic 205–180 Ma magmatic quiescence (Zhou et al., 2006a). More importantly, these bimodal intrusive rocks are products of a continental extensional environment, signifying the initiation of the early Jurassic anorogenic extensional magmatism at ca. 194 Ma in SE China. The present study thus lends further support to the model of Li and Li (2007) that the early Jurassic anorogenic magmatism was most likely triggered by upwelling of asthenopheric mantle, with basaltic underplating and/or intrusion providing the heat source and pivotal mantle-derived material for the generation of the A-type granites.

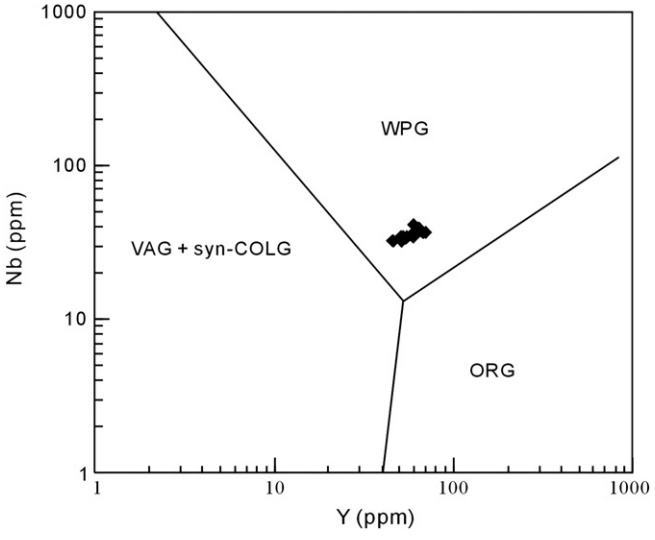

Fig. 14. Nb vs. Y diagram of Pearce et al. (1984) showing that the Wengong granites are plotted exclusively into the field of within-plate granites (WPG).

6. Conclusions

The following conclusions are drawn on the basis of the present study:

(1) SHRIMP and Cameca SIMS zircon U–Pb dating results indicate that the gabbros from the Xialan mafic–ultramafic intrusion and the granites from the Wengong pluton were emplaced at 194 ± 1 Ma and 192 ± 1 Ma, respectively, suggesting that they were formed during a narrow time interval.

(2) The Xialan gabbros exhibit positive $\varepsilon_{Nd}(i)$ and low I_{Sr} values, implying that the parental magma of the mafic–ultramafic intrusion is a high-Ti subalkaline basaltic magma derived from melting of a depleted asthenospheric mantle source. The mafic–ultramafic intrusion was thereafter formed by fractional crystallization of the parental magma combined with variable degrees of crustal contamination.

(3) The Wengong granites show the features of peraluminous A_2-type granites. The granites were most likely formed by partial melting of the pre-existing Paleoproterozoic lower crust, and then mixed with varying amounts of the early Jurassic mantle-derived basaltic magmas. The magmas parental to the Wengong granites would further experience extensive magmatic differentiation to account for the geochemical characteristics of the granitic pluton.

(4) The generation of the Xialan mafic–ultramafic intrusion and Wengong granitic pluton indicates that ca. 194 Ma is an important onset time of the early Jurassic anorogenic magmatism in SE China, which was most likely formed in response to the break-up and foundering of the subducted flat-slab beneath the SE China continent.

Acknowledgements

We appreciate the assistances of G.F. Zhou, W.Q. Zheng, and S.R. Liu in electron microprobe analysis, D.Y. Liu, B. Song, Y.S. Wan, Z.Q. Yang, Y.R. Shi and H. Tao in SHRIMP dating, Y. Liu, and Q.L. Li in SIMS dating, C.X. Feng in major element analyses by XRF, J. Hu, Y.R. Cai, Y. Huang for trace element analyses by ICP-MS, Z.Y. Chu, and C.F. Li for Nd–Sr isotope analyses by TIMS. The paper has benefited from review comments of the editor N. Eby and two anonymous reviewers. This work is supported jointly by the National Basic Research Program of China (2007CB411403 and 2007CB411401), the NSFC (Grants 40673031, 40730420, 40673030), and a Special Research Fund of the SKLOG, IGCAS.

Appendix A. Supplementary data

Supplementary data associated with this article can be found, in the online version, at doi:10.1016/j.lithos.2010.07.005.

References

Arth, J.G., 1976. Behaviour of trace elements during magmatic processes: a summary of theoretical models and their applications. Journal of Research of the U.S. Geological Survey 4, 41–47.

Barbarin, B., 1999. A review of the relationships between granitoid types, their origins and their geodynamic environments. Lithos 46, 605–626.

Beard, J.S., Lofgren, G.E., 1991. Dehydration melting and water saturated melting of basaltic and andesitic greenstones and amphibolites at 1, 3 and 6. 9 kbar. Journal of Petrology 32, 365–401.

Bonin, B., 1996. A-type granite ring complex: mantle origin through crustal filters and the anorthosite-rapakivi magmatism connection. In: Demaiffe, D. (Ed.), Petrology and Geochemistry of Magmatic Suites of Rocks in the Continental and Oceanic Crusts: Brussels, Belgium. Université Libre de Bruxelles, Royal Museum for Central Africa (Tervuren), pp. 201–218.

Borg, L.E., Clynne, M.A., 1998. The petrogenesis of felsic calc-alkaline magmas from the southernmost Cascades, California: origin by partial melting of basaltic lower crust. Journal of Petrology 39, 1197–1222.

Boynton, W.V., 1984. Geochemistry of the rare earth elements: meteorite studies. In: Henderson, P. (Ed.), Rare Earth Element Geochemistry. Elservier, pp. 63–114.

Cabanis, B., Lecolle, M., 1989. Le diagramme La/10–Y/15–Nb/8: un outil pour la discrimination des series volcaniques et la mise en evidence des procesus de melange et/ou de contamination crutale. Comptes Rendus de l'Académie des Sciences Series II 309, 2023–2029.
Charvet, J., Lapierre, H., Yu, Y., 1994. Geodynamic significance of the Mesozoic volcanism of southeastern China. Journal of Southeast Asian Earth Sciences 68, 387–396.
Chen, P.R., Zhang, B.T., Kong, X.G., Cai, B.C., Ling, H.F., Ni, Q.S., 1998. Geochemical characteristics and tectonic implication of Zhaibei A-type granitic intrusive in south Jiangxi province. Acta Petrologica Sinica 14, 289–298 (in Chinese with English abstract).
Chen, P.R., Kong, X.G., Wang, Y.X., Ni, Q.S., Zhang, B.T., Ling, H.F., 1999. Rb–Sr isotopic dating and significance of early Yanshanian bimodal volcanic–intrusive complex from southern Jiangxi Province, SE China. Geological Journal of China Universities 5, 378–382 (in Chinese with English abstract).
Chen, Z.Q., Li, W.H., Guo, L., 2001. Granite of Proterozoic eon found in northeast Guangdong. Guangdong Geology 16 (4), 16–21 (in Chinese with English abstract).
Chen, Z.Q., Wu, J.T., Kang, Y.G., 2002b. Characteristics of the Xianlan intrusion of basic–intermediate composition in Xingning. Guangdong Geology 17 (1), 38–43 (in Chinese with English abstract).
Chen, Z.Q., Li, W.H., Guo, L., 2002c. Geological and geochemical characteristics of Wengong pluton and the Relation with Xianlan pluton in Xingning. Guangdong Geology 17 (3), 15–20 (in Chinese with English abstract).
Chen, P.R., Hua, R.M., Zhang, P.T., Lu, J.J., Fan, C.F., 2002a. Early Yanshanian post-orogenic granitoids in the Nanling region: petrological constraints and geodynamic settings. Science in China Series D 45, 755–768.
Chen, P.R., Zhou, X.M., Zhang, W.L., Li, H.M., Fan, C.F., Sun, T., Chen, W.F., Zhang, M., 2005. Petrogenesis and significance of early Yanshanian syenite–granite complex in eastern Nanling Range. Science in China Series D 48, 912–924.
Chen, C.-H., Lee, C.-Y., Shinjo, R., 2008. Was there Jurassic paleo-Pacific subduction in South China?: constraints from $^{40}Ar/^{39}Ar$ dating, elemental and Sr–Nd–Pb isotopic geochemistry of the Mesozoic basalts. Lithos 106, 83–92.
Collins, W.J., Beams, S.D., White, A.J.R., Chappell, B.W., 1982. Nature and origin of A-type granites with particular reference to southeastern Australia. Contributions to Mineralogy and Petrology 80, 189–200.
Compston, W., Williams, I.S., Kirschvink, J.L., Zhang, Z., Ma, G., 1992. Zircon U–Pb ages for the Early Cambrian time-scale. Journal of the Geological Society, London 149, 171–184.
Cox, K.G., Bell, J.D., Pankhurst, R.J., 1979. The Interpretation of Igneous Rocks. Allen and Unwin, London, UK. 450 pp.
De la Roche, H., Leterrier, J., Granclaude, P., Marchal, M., 1980. A classification of volcanic and plutonic rocks using R1R2-diagram and major-element analyses—its relationships with current nomenclature. Chemical Geology 29, 183–210.
Ding, X., Chen, P.R., Chen, W.F., Huang, H.Y., Zhou, X.M., 2006. Single zircon LA-ICPMS U–Pb dating of Weishan granite (Hunan, South China) and its petrogenetic significance. Science in China Series D 49, 816–827.
Eby, G.N., 1992. Chemical subdivision of the A-type granitoids: petrogenetic and tectonic implications. Geology 20, 641–644.
Ewart, A., Milner, S.C., Armstrong, R.A., Duncan, A.R., 1998. Etendeka volcanism of the Goboboseb Mountains and Messum igneous complex, Namibia. Part I: geochemical evidence of early Cretaceous Tristan Plume melts and the role of crustal contamination in the Parana–Etendeka CFB. Journal of Petrology 39, 191–225.
Frost, B.R., Barnes, C.G., Collins, W.J., Arculus, R.J., Ellis, D.J., Frost, C.D., 2001. A geochemical classification for granitic rocks. Journal of Petrology 42, 2033–2048.
Garland, F., Turne, S., Hawkesworth, C., 1996. Shifts in the source of the Paraná basalts through time. Lithos 37, 223–243.
Gilder, S.A., Keller, G.R., Luo, M., Goodell, P.C., 1991. Timing and spatial distribution of rifting in China. Tectonophysics 197, 225–243.
Guffanti, M., Clynne, M.A., Muffler, L.J.P., 1996. Thermal and mass implications of magmatic evolution in the Lassen volcanic region, California, and constraints on basalt influx to the lower curst. Journal of Geophysical Research 101, 3001–3013.
Han, B.F., Wang, S.G., Jahn, B.M., Hong, D.W., Kagami, H., Sun, Y.L., 1997. Depleted-mantle source for the Ulungur River A-type granites from North Xinjiang, China: geochemistry and Nd–Sr isotopic evidence, and implications for Phanerozoic crustal growth. Chemical Geology 138, 135–159.
Hay, D.E., Wendlandt, R.F., 1995. The origin of Kenya rift plateau type phonolites: results of high-pressure/high-temperature experiments in the system phonolite–H2O and phonolite–H2O–CO2. Journal of Geophysical Research 100, 401–410.
Hoffman, P.F., 1989. Speculations on Laurentia's first gigayear (2.0 to 1.0 Ga). Geology 17, 135–138.
Hofmann, A.W., Jochum, K.P., 1996. Source characteristics derived from very incompatible trace elements in Mauna Loa and Mauna Kea basalts, Hawaii Scientific Drilling Project. Journal of Geophysical Research 101 (B5), 11831–11839.
Holloway, N.H., 1982. North Palawan Block, Philippines — its relation to Asian Mainland and role in evolution of South China Sea. AAPG Bulletin 66, 1355–1383.
Huppert, H.E., Sparks, R.S.J., 1988. The generation of granitic magmas by intrusion of basalt into continental crust. Journal of Petrology 29, 599–624.
Institute of Guangdong geological survey (IGGS), 2002. 1:50000 geological map of the Luogang Town (G50 E 022007) in the Xingning County, Guangdong province.
Jahn, B.M., Chen, P.Y., Yen, T.P., 1976. Rb–Sr ages of granitic rocks in southeastern China and their tectonic significance. Geological Society of America 86, 763–776.
Jahn, B.M., Zhou, X.H., Li, J.L., 1990. Formation and tectonic evolution of southeastern China and Taiwan: isotopic and geochemical constraints. Tectonophysics 1990 (183), 145–160.
Jahn, B.M., Wu, F.Y., Lo, C.H., Tsai, C.H., 1999. Crust–mantle interaction induced by deep subduction of the continental crust: geochemical and Sr–Nd isotopic evidence from post-collisional mafic–ultramafic intrusions of the northern Dabie complex, central China. Chemical Geology 157, 119–146.
Jiang, Y.H., Jiang, S.Y., Dai, B.Z., Liao, S.Y., Zhao, K.D., Ling, H.F., 2009. Middle to late Jurassic felsic and mafic magmatism in southern Hunan province, southeast China: implications for a continental arc to rifting. Lithos 107, 185–204.
Jin, W., Sun, D., 1997. Deep Crustal Structure and its Evolution of South China. Geological Publishing House, Beijing. 175 pp. (in Chinese with English summary).
King, P.L., White, A.J.R., Chappell, B.W., Allen, C.M., 1997. Characterization and origin of aluminous A-type granites from the Lachlan Fold Belt, southeastern Australia. Journal of Petrology 38, 371–391.
Kong, X.G., Chen, P.R., Zhang, B.T., 2000. Confirmation of A-type volcanics in Baimianshi and Dongkeng basin, south Jiangxi province and their geological implication. Geochimica 29, 521–524 (in Chinese with English abstract).
Lan, C.Y., Jahn, B.M., Mertzman, S.A., Wu, T.W., 1996. Subduction-related granitic rocks of Taiwan. Journal of Southeast Asian Earth Sciences 14, 11–28.
Lapierre, H., Jahn, B.M., Charvet, J., Yu, Y.W., 1997. Mesozoic magmatism in Zhejiang Province and its relation with the tectonic activities in SE China. Tectonophysics 274, 321–338.
Li, X.H., 1997. Timing of Cathaysia Block formation: constraints from SHRIMP U–Pb zircon geochronology. Episodes 20, 188–192.
Li, X.H., 2000. Cretaceous magmatism and lithospheric extension in Southeast China. Journal of Asian Earth Sciences 18, 293–305.
Li, Z.X., Li, X.H., 2007. Formation of the 1300 km-wide intracontinental orogen and post-orogenic magmatic province in Mesozoic South China: a flat-slab subduction model. Geology 35, 179–182.
Li, X.H., McCulloch, M.T., 1998. Geochemical characteristics of Cretaceous mafic dikes from northern Guangdong, SE China: Age, origin and tectonic significance. In: Flower, M.F.J., Chung, S.L., Lo, C.H., Lee, T.-Y. (Eds.), Mantle Dynamics and Plate Interaction in East Asia. : AGU Geodynamics, 27. Washington, DC, pp. 405–419.
Li, Z.X., Li, X.H., Kinny, P.D., Wang, J., 1999. The breakup of Rodinia: did it start with a mantle plume beneath South China? Earth and Planetary Science Letters 173, 171–181.
Li, X.H., Sun, M., Wei, G.J., Liu, Y., Lee, C.Y., Malpas, J., 2000. Geochemical and Sm–Nd isotopic study of amphibolites in the Cathaysia Block, southeastern China: evidence for an extremely depleted mantle in the Paleoproterozoic. Precambrian Research 102, 251–262.
Li, X.H., Chen, Z.G., Liu, D.Y., Li, W.X., 2003. Jurassic gabbro–granite–syenite suites from southern Jiangxi province, SE China: age, origin, and tectonic significance. International Geology Revview 45, 898–921.
Li, X.H., Chung, S.L., Zhou, H.W., Lo, C.H., Liu, Y., Chen, C.H., 2004. Jurassic intraplate magmatism in southern Hunan–eastern Guangxi: $^{40}Ar/^{39}Ar$ dating, geochemistry, Sr–Nd isotopes and implications for the tectonic evolution of SE China. Aspects of the Tectonic Evolution of China: In: Malpas, J., Fletcher, C.J., Aitchison, J.C., Ali, J. (Eds.), Geological Society, London, Special Publications, vol. 226, pp. 193–216.
Li, W.X., Li, X.H., Li, Z.X., 2005. Neoproterozoic bimodal magmatism in the Cathaysia Block of South China and its tectonic significance. Journal of Asian Earth Sciences 136, 51–66.
Li, X.H., Li, Z.X., Li, W.X., Wang, Y.J., 2006. Initiation of the Indosinian Orogeny in South China: evidence for a Permian magmatic arc on the Hainan Island. The Journal of Geology 114, 341–353.
Li, X.H., Li, Z.X., Li, W.X., Liu, Y., Yuan, C., Wei, G.J., Qi, C.S., 2007a. U–Pb zircon, geochemical and Sr–Nd–Hf isotopic constraints on age and origin of Jurassic I- and A-type granites from central Guangdong, SE China: a major igneous event in response to foundering of a subducted flat-slab? Lithos 96, 186–204.
Li, X.H., Li, W.X., Li, Z.X., 2007b. On the genetic classifications and tectonic implications of the Early Yanshanian granitoids in the Nanling Range of South China. Chinese Science Bulletin 52, 1873–1885.
Li, X.H., Liu, Y., Li, Q.L., Guo, C.H., Chamberlain, K.R., 2009a. Precise determination of Phanerozoic zircon Pb/Pb age by multi-collector SIMS without external standardization. Geochemistry Geophysics Geosystems 10, Q04010. doi:10.1029/2009GC002400.
Li, X.H., Li, W.X., Wang, X.C., Li, Q.L., Liu, Y., Tang, G.Q., 2009b. Role of mantle-derived magma in genesis of early Yanshanian granites in the Nanling Range, South China: in situ zircon Hf–O isotopic constraints. Science in China Series D 52, 1262–1278.
Li, Q.L., Li, X.H., Liu, Y., Tang, G.Q., Yang, J.H., Zhu, W.G., 2010. Precise U–Pb and Pb–Pb dating of Phanerozoic baddeleyite by SIMS with oxygen flooding technique. Journal of Analytical Atomic Spectrometry. doi:10.1039/B923444F.
Lightfoot, P.C., Hawkesworth, C.J., Hergt, J., Naldrett, A.J., Gorbachev, N.S., Fedorenko, V.A., Doherty, W., 1993. Remobilisation of the continental lithosphere by a mantle plume: major-, trace-element, and Sr-, Nd-, and Pb-isotope evidence from picritic and tholeiitic lavas of the Noril'sk District, Siberian Trap, Russia. Contributions to Mineralogy and Petrology 114, 171–188.
Loucks, R.R., 1990. Discrimination of ophiolitic from nonophiolitic ultramafic–mafic allochthons in orogenic belts by the Al/Ti ratio in clinopyroxene. Geology 18, 346–349.
Lugmair, G.W., Harti, K., 1978. Lunar initial $^{143}Nd/^{144}Nd$: differential evolution of the lunar crust and mantle. Earth and Planetary Science Letters 39, 349–357.
Martin, H., Bonin, B., Capdevila, R., Jahn, B.M., Lameyre, J., Wang, Y., 1994. The Kuiqi peralkaline granitic complex (SE China): petrology and geochemistry. Journal of Petrology 35, 983–1015.
Nedelec, A., Stephens, W.E., Fallick, A.E., 1995. The Panafrican stratoid granites of Madagascar: alkaline magmatism in a postcollisional extensional setting. Journal of Petrology 36, 1367–1391.
Ormerod, D.S., Hawkesworth, C.J., Rogers, N.W., Leeman, W.P., Menzies, M.A., 1988. Tectonic and magmatic transitions in the western Great Basin, USA. Nature 333, 349–353.

Paces, J.B., Bell, K., 1989. Non-depleted sub-continental mantle beneath the Superior Province of the Canadian Shield: Nd–Sr isotopic and trace element evidence from midcontinent rift basalts. Geochimica et Cosmochimica Acta 53, 2023–2035.
Pearce, J.A., Harris, N.B.W., Tindle, A.G., 1984. Trace element discrimination diagrams for the tectonic interpretation of granitic rocks. Journal of Petrology 25, 956–983.
Peate, D.W., Hawkesworth, C.J., Mantovani, M.S.M., 1992. Chemical stratigraphy of the Parana lavas South America: classification of magma-types and their spatial distribution. Bulletin of Volcanology 55, 119–139.
Peccerillo, A., Barberio, M.R., Yirgu, G., Ayalew, D., Barbieri, M., Wu, T.W., 2003. Relationships between mafic and peralkaline silicic magmatism in continental rift settings: a petrological, geochemical and isotopic study of the Gedemsa Volcano, central Ethiopian rift. Journal of Petrology 44, 2003–2032.
Qi, L., Hu, J., Grégoire, D.C., 2000. Determination of trace elements in granites by inductively coupled plasma mass spectrometry. Talanta 51, 507–513.
Riley, T.R., Leat, P.T., Pankhurst, R.J., Harris, C., 2001. Origin of large volume rhyolitic volcanism in the Antarctic Peninsula and Patagonia by crustal melting. Journal of Petrology 42, 1043–1065.
Rogers, J.J.W., Greenberg, J.K., 1990. Late-orogenic, post-orogenic, and anorogenic granites: distinction by major element and trace element chemistry and possible origins. Journal of Petrology 98, 291–309.
Rollinson, 1993. Using Geochemical Data: Evolution, Presentation, Interpretation. Longman scientific and Technical. 352 pp.
Rudnick, R.L., Fountain, D.M., 1995. Nature and composition of the continental crust: a lower crustal perspective. Reviews of Geophysics 33, 267–309.
Sewell, R.J., Campbell, S.D.G., 1997. Geochemistry of coeval Mesozoic plutonic and volcanic suites in Hong Kong. Journal of the Geological Society, London 154, 1053–1066.
Song, B., Zhang, Y.H., Wan, Y.S., Jian, P., 2002. Mount making and procedure of the SHRIMP dating. Geological Review 48, 26–30 (Suppl., in Chinese with English abstract).
Stacey, J.S., Kramers, J.D., 1975. Approximation of terrestrial lead isotope evolution by a two-stage model. Earth and Planetary Science Letters 26, 207–221.
Steiger, R.H., Jäger, E., 1977. Subcommission on geochronology: convention on the use of decay constants in geo- and cosmochronology. Earth and Planetary Science Letters 36, 359–362.
Sun, S.-S., McDonough, W.F., 1989. Chemical and isotopic systematics of oceanic basalts: implications for mantle composition and processes. Magmatism in the Ocean Basins: In: Saunders, A.D., Norry, M.J. (Eds.), Geological Society, London, Special Publications, no. 42, pp. 313–345.
Sun, Q.H., Yang, Z.L., Chen, Y., Li, Q.H., Xing, G.F., 2002. Metallogenic geology of the Xianlan–Yonghe vanadic titanomagnetite deposit belt in Xingning of Guangdong province. Resources Survey and Environment 23, 266–271 (in Chinese with English abstract).
Sylvester, P.J., 1989. Post-collisional alkaline granites. Journal of Petrology 97, 261–280.
Thy, P., Beard, J.S., Logfren, G.E., 1990. Experimental constraints on the origin of Icelandic rhyolites. Journal of Petrology 98, 417–421.
Turner, S.P., Foden, J.D., Morrison, R.S., 1992. Derivation of some A-type magmas by fractionation of basaltic magma: an example from the Padthaway Ridge, South Australia. Lithos 28, 151–179.
Wan, Y.S., Liu, D.Y., Wilde, S.A., Cao, J.J., Chen, B., Dong, C.Y., Song, B., Du, L.L., 2010. Evolution of the Yunkai Terrane, South China: evidence from SHRIMP zircon U–Pb dating, geochemistry and Nd isotope. Journal of Asian Earth Sciences 37, 140–153.
Wang, W.H., 1999. Reappraisal of the Xianlan weathering crust vanadic titanomagnetite deposit in Xingneng. Guangdong Geology 14 (4), 22–29 (in Chinese with English abstract).
Wang, Y.J., Fan, W.M., Guo, F., Peng, T.P., Li, C.W., 2003. Geochemistry of Mesozoic mafic rocks adjacent to the Chenzhou–Linwu fault, South China: implications for the lithospheric boundary between the Yangtze and Cathaysia Blocks. International Geology Review 45, 263–286.
Wang, Y.J., Fan, W.M., Peng, T.P., Guo, F., 2004. Early Mesozoic OIB-type alkaline basalts in central Jiagnxi Province and its tectonic implication. Geochimica 33, 109–117 (in Chinese with English abstract).
Wang, Q., Li, J.W., Jian, P., Zhao, Z.H., Xiong, X.L., Bao, Z.W., Xu, J.F., Li, C.F., Ma, J.L., 2005a. Alkaline syenites in eastern Cathaysia (South China): link to Permian–Triassic transtension. Earth and Planetary Science Letters 230, 339–354.
Wang, Y.J., Fan, W.M., Peng, T.P., Guo, F., 2005b. Elemental and Sr–Nd isotopic systematics of the early Mesozoic volcanic sequence in southern Jiangxi Province, South China: petrogenesis and tectonic implications. International Journal of Earth Sciences 94, 53–65.
Watson, E.B., Capobianco, C.J., 1981. Phosphorus and the rare earth elements in felsic magmas an assessment of the role of apatite. Geochimica et Cosmochimica Acta 45, 2349–2358.
Watson, E.B., Harrison, T.M., 1983. Zircon saturation revisited: temperature and composition effects in a variety of crustal magma types. Earth and Planetary Science Letters 64, 295–304.
Whalen, J.B., Currie, K.L., Chappell, B.W., 1987. A-type granites: geochemical characteristics, discrimination and petrogenesis. Contributions to Mineralogy and Petrology 95, 407–419.
Wiedenbeck, M., Alle, P., Corfu, F., Griffin, W.L., Meier, M., Oberli, F., Vonquadt, A., Roddick, J.C., Speigel, W., 1995. Three natural zircon standards for U–Th–Pb, Lu–Hf, trace-element and REE analyses. Geostandard Newsletter 19, 1–23.
Winchester, J.A., Floyd, P.A., 1976. Geochemical magma type discrimination: application to altered and metamorphosed igneous rocks. Earth and Planetary Science Letters 45, 326–336.
Wu, F.Y., Sun, D.Y., Li, H.M., Jahn, B.M., Wilde, S.A., 2002. A-type granites in northeastern China: age and geochemical constraints on their petrogenesis. Chemical Geology 187, 143–173.
Xie, M.M., Liu, C.G., Li, S., Liu, C.G., Li, S., 2001. Geological feature of Xiakengzi pluton of Anyuan, south and geological significance of Pb–Pb isotopic age of zircon. Jiangxi Geology 15, 256–269 (in Chinese with English abstract).
Xing, G.F., Yang, Z.L., Sun, Q.H., Shen, J.L., Tao, K.L., 2001. Bull. Early Jurassic layered mafic–ultramafic intrusions in Meizhou, Guangdong province. Bulletin of Mineralogy, Petrology and Geochemistry 20, 172–175 (in Chinese with English abstract).
Xing, G.F., Yang, Z.L., Mao, J.R., Shu, L.S., Shen, J.L., Sun, Q.H., Chen, Y., Tao, K.Y., 2002. Characteristics of early Jurassic igneous rocks on the continental margin of southeastern China and their tectonic significance. Geological Bulletin of China 21, 384–391 (in Chinese with English abstract).
Xu, Y.G., Chung, S.L., Jahn, B.M., Wu, G.Y., 2001. Petrologic and geochemical constraints on the petrogenesis of Permian–Triassic Emeishan flood basalts in southwestern China. Lithos 58, 145–168.
Yu, X.Q., Di, Y.J., Wu, G.G., Zhang, D., Zheng, Y., Dai, Y.P., 2009. The early Jurassic magmatism in northern Guangdong province, southeastern China: constraints from SHRIMP zircon U–Pb dating of Xialan complex. Science in China Series D 52, 471–483.
Zhou, X.M., Li, W.X., 2000. Origin of Late Mesozoic igneous rocks in Southeastern China: implications for lithosphere subduction and underplating of mafic magmas. Tectonophysics 326, 269–287.
Zhou, J.C., Jiang, S.Y., Wang, X.L., Yang, J.H., 2005. Re–Os isochron age of Fankeng basalts from Fujian of SE China and its geological significance. Geochemical Journal 39, 497–502.
Zhou, X.M., Sun, T., Shen, W.Z., Shu, L.S., Niu, Y.L., 2006b. Petrogenesis of Mesozoic granitoids and volcanic rocks in South China: a response to tectonic evolution. Episodes 29, 26–33.
Zhou, J.C., Jiang, S.Y., Wang, X.L., Yang, J.H., Zhang, M.Q., 2006a. Study on lithogeochemistry of Middle Jurassic basalts from southern China represented by the Fankeng basalts from Yongding of Fujian Province. Science in China Series D 49, 1020–1031.